We are IntechOpen, the world's leading publisher of Open Access books Built by scientists, for scientists

6,900
Open access books available

185,000
International authors and editors

200M
Downloads

Our authors are among the

154
Countries delivered to

TOP 1%
most cited scientists

12.2%
Contributors from top 500 universities



WEB OF SCIENCE™

Selection of our books indexed in the Book Citation Index in Web of Science™ Core Collection (BKCI)

Interested in publishing with us?
Contact book.department@intechopen.com

Numbers displayed above are based on latest data collected.
For more information visit www.intechopen.com



1

CO_2 Laser Photoacoustic Spectroscopy: I. Principles

Dan C. Dumitras, Ana Maria Bratu and Cristina Popa
Department of Lasers, National Institute for Laser, Plasma, and Radiation Physics, Bucharest Romania

1. Introduction

Laser photoacoustic spectroscopy (LPAS) has emerged over the last decade as a very powerful investigation technique, capable of measuring trace gas concentrations at ppmV (parts per million by volume), or even sub-ppbV (parts per billion by volume) level. Recent achievements in this field have made it possible to fully characterize the method and improve the design of instrument components in view of the task they are expected to fulfill.

1.1 Historical remarks

The photoacoustic (PA) (formerly also known as optoacoustic) effect consisting in sound generation from the interaction of light and matter was discovered by Alexander Graham Bell (Bell, 1880). He noticed that focused intensity-modulated light (chopped sunlight) falling on an optically absorbing solid substance produced an audible sound. In the next year, light absorption was detected through its accompanying acoustic effect not only in solids, but also in liquids and gases by Bell (Bell, 1881), Tyndall (Tyndall, 1881), Röntgen (Röntgen, 1881), and Preece (Preece, 1881). They found the sound was stronger when the substance was placed in a sample cell (then called "photophone" and later "spectrophone"). It was Bell again that first described the resonant amplification of the PA signal (Bell, 1881). The PA effect was also investigated at different light wavelengths. Bell and Preece were among the first to notice a PA signal for an aerosol when they experimented with cigar smoke. The advances of photoacoustic spectroscopy up to the invention of the laser were reviewed by Kaiser in 1959 (Kaiser, 1959).

Over the last five decades, technological developments in the field of lasers and high-sensitivity pressure detection systems (microphones and electronics) have contributed to the substantial progress of photoacoustic spectroscopy. The introduction of laser light sources emitting highly monochromatic and collimated intense beams have opened up new areas of research. Lasers provide the advantage of high spectral power density owing to their intrinsic narrow linewidth. This laser linewidth is usually much smaller than the molecular absorption linewidth (GHz region at atmospheric pressure), and therefore it is not an important issue in most measurements. A true revival of PA spectroscopy was due to Kerr and Atwood (Kerr & Atwood, 1968), who made the earliest experiments with a laser illuminated PA detector in 1968, and Kreuzer (Kreuzer, 1971), who first measured gas

concentrations using a PA detector and a laser in 1971. Later experiments by Kreuzer and collaborators (Kreuzer & Patel, 1971; Kreuzer et. al., 1972) effectively demonstrated the extremely high sensitivity attainable by this method. To improve the detection of atmospheric pollutants, Dewey et al. (Dewey et. al., 1973) have used in 1973 an acoustic resonance chamber and have reached amplification factors higher than 100. In 1977, the feasibility of *in situ* aerosol measurements, which were important for atmospheric applications, was first reported by Bruce and Pinnick (Bruce & Pinnick, 1977) and Terhune and Anderson (Terhune & Anderson, 1977). Subsequently, many experimental and theoretical works have been reported in the literature, proving the applicability of the method not only in spectroscopy, but also in various fields of physics, chemistry, biology, medicine, and engineering. The potential of laser photoacoustic spectroscopy has been discussed in several review articles (Patel & Tam, 1981; West, 1983; Hess, 1983; Tam, 1986; Sigrist, 1986, 2003; Meyer & Sigrist, 1990; Harren & Reuss, 1997; Harren et al., 2000; Miklos et al., 2001; Schmid, 2006) and books (Pao, 1977; Rosencwaig, 1980; Zharov & Letokhov, 1986; Hess, 1989; Mandelis, 1992, 1994; Bicanic, 1992; Gusev & Karabutov, 1993; Sigrist, 1994; Mandelis & Hess, 1997).

1.2 Features of a gas sensor

The most important features of a gas sensor include high sensitivity and selectivity, large dynamic range, high accuracy and precision, good temporal resolution, ease of use, versatility, reliability, robustness, and multicomponent capability. Gas chromatographs are neither sensitive nor fast enough. Although there is no ideal instrument that would fulfill all the requirements mentioned above, a spectroscopic method and particularly the simple setup of LPAS provide several unique advantages, notably the multicomponent capability, high sensitivity and selectivity, wide dynamic range, immunity to electromagnetic interferences, convenient real time data analysis, operational simplicity, relative portability, relatively low cost per unit, easy calibration, and generally no need for sample preparation. LPAS is primarily a calorimetric technique and, as such, differs completely from other previous techniques, as the absorbed energy can be determined directly, instead of via measurement of the intensity of the transmitted or backscattered radiation. In conjunction with tunable lasers, *in situ* monitoring of many substances occurring at ppbV or even pptV (parts per trillion by volume) concentrations is a routine task today. PA detection provides not only high sensitivity but also the necessary selectivity for analyzing multicomponent mixtures by the use of line-tunable IR lasers, e.g., CO lasers (Sigrist et al., 1989) or CO_2 lasers (Meyer & Sigrist, 1990).

CO_2 laser photoacoustic spectroscopy offers a sensitive technique for detection and monitoring of trace gases at low concentrations. The CO_2 laser is of special interest, as it ensures high output power in a wavelength region (9-11 μm) where more than 250 molecular gases/vapors of environmental concern for atmospheric, industrial, medical, military, and scientific spheres exhibit strong absorption bands (Hubert, 1983). This laser, however, can be only stepwise tuned when operated in cw (continuous wave). Nevertheless, it is an ideal source to push the sensitivity of PA gas detection into the concentration range of ppbV or even lower. Instruments based on LPAS have nearly attained the theoretical noise equivalent absorption detectivity of 10^{-10} cm^{-1} in controlled laboratory conditions (Harren et al., 1990). This high sensitivity cannot be achieved in real detection conditions due to the coherent photoacoustical background signal and interfering background absorption of normal atmospheric constituents.

At present many research groups are actively involved in the development of LPAS systems for various applications in different disciplines, including nondestructive evaluation of materials, environmental analysis, agricultural, biological, and medical applications, investigation of physical processes (phase transitions, heat and mass transfer, kinetic studies), and many others. Our facility, which was originally designed for ethylene (C_2H_4) analysis at the low ppb level, is adaptable with minor modifications to a broad range of gases and vapors having absorption spectra in the infrared (IR).

2. Basic principles

2.1 Linear laser spectroscopy methods

A gaseous molecule that absorbs electromagnetic radiation is excited to a higher electronic, vibrational or rotational quantum state. The excited state loses its energy by radiation processes, such as spontaneous (fluorescence) or stimulated emission, and/or by collisional relaxation, in which energy is converted into translational energy. Radiative emission and chemical reactions do not play an important role in the case of vibrational excitation, because the radiative lifetimes of the vibrational levels are long compared with the time needed for collisional deactivation at pressures used in photoacoustics (~1 bar), and the photon energy is too small to induce chemical reactions. Thus, in practice the absorbed energy is completely released via either fluorescence (at low pressures) or collisions. The latter give rise to a gas temperature increase due to energy transfer to translation as heat, appearing as translational (kinetic) energy of the gas molecules. The deposited heat power density is proportional to the absorption coefficient and incident light intensity. The nonradiative relaxation process occurs when the relaxation time can compete with the radiative lifetime of the excited energy levels. Radiative decay has a characteristic lifetime of 10^{-7} s at visible wavelengths as compared with 10^{-2} s in IR at 10 μm. For nonradiative decay these values depend on pressure (the decay time τ is inversely proportional to pressure) and may vary strongly at atmospheric pressures (10^{-3}-10^{-8} s) depending on the gas nature and the involved energy level.

There are three techniques of linear laser spectroscopy, based on measurement of different physical quantities:

- the absorption method and the cavity ringdown spectroscopy (intensity);
- the radiative method (fluorescence); and
- the photothermal (calorimetric) method (pressure, temperature).

The most important optical process, as far as spectroscopic trace gas detection is concerned, is based on the extinction of radiation by molecular absorption. The absorption features and strengths specific of each molecule make it possible to identify trace gases and determine their concentrations. Absorption coefficients are typically on the order of 1 cm^{-1} (one wave number). The absorption of trace gas molecules in a gas mixture may be monitored by detecting the attenuation of the laser beam over a fixed absorption path length L. According to the Beer-Lambert law, the transmitted laser power in the absence of saturation is given by:

$$P(L) = P(0)\exp(\alpha_p L) = P(0)\exp(\alpha c L), \quad (1)$$

where $P(0)$ and $P(L)$ are the laser powers before and after the absorption cell, respectively; α_p (cm^{-1}) is the absorption coefficient at a given pressure of the gas at a specific laser

wavelength: $\alpha_p = \alpha c$; α (cm^{-1} atm^{-1}) is the gas absorption coefficient (the absorption coefficient normalized to unit concentration), and c (atm) is the trace gas concentration. Also, $\alpha_p = N_{tot}\sigma$, where σ (cm^2) is the absorption cross section per molecule and N_{tot} = 2.5×10^{19} molecules cm^{-3} is the number of absorbing molecules per cubic centimeters at 1013 mbar and 20°C. It results:

$$c = -\frac{1}{\alpha L}\ln\frac{P(L)}{P(0)} = -\frac{1}{\alpha L}\ln\left(1-\frac{\Delta P}{P(0)}\right) \cong \frac{1}{\alpha L}\frac{\Delta P}{P(0)}, \tag{2}$$

which is valid for $\Delta P/P(0) << 1$ (optically thin sample), where $\Delta P = P(0) - P(L)$. For a given L, the detection limit is given by the smallest relative change $\Delta P_{min}/P(0)$ that can be measured in the transmitted signal. For dilute mixtures and modest absorption path lengths, the desired signal is the small difference between two large values so that high quantitative accuracies in signal intensities are required. The most sensitive method employs frequency modulation and harmonic detection. The sensitivity depends on the linewidth, and for atmospherically broadened lines, Reid et al. (Reid et al., 1978) have reached $\Delta P_{min}/P(0) \cong 10^{-5}$ in a diode laser spectrometer (1050-1150 cm^{-1}). With a path length of 100 m, the result is a sensitivity of 10^{-9} cm^{-1}, which corresponds to concentrations of 3 ppbV of a weakly absorbing molecule such as SO_2 (ν_1 band), or 0.01 ppbV of a strongly absorbing molecule such as CO. Assuming the same detectable attenuation $\Delta P_{min}/P(0) \cong 10^{-5}$, a path length L = 1 m, and an absorption coefficient α = 30.4 $cm^{-1}atm^{-1}$ (typical of fundamental absorption in the mid-IR), one obtains a minimum detectable absorption coefficient $\alpha_p = 10^{-7}$ cm^{-1}. This number corresponds to a concentration of 3.3 ppbV at atmospheric pressure. Conventional absorption techniques, which require precise measurements of the difference between two nearly equal signals are, however, unable to realize the full potential of the higher power levels now attainable. Improvement may be obtained by: increasing the path length L in a multipass or intracavity arrangement, or using wavelength modulation, i.e., by modulating the wavelength of the incident intensity across a molecular absorption line. In multipass transmission absorption spectroscopy, a multipass transmission cell (White cell) filled with analyte gas with mirrors at each end is used. The beam is folded back and forth through the cell, creating an extended yet defined optical path length within a confined space.

Cavity ringdown spectroscopy confines gas in an optically reflective cavity where laser radiation is introduced. Radiation amplitude decays at a certain rate in the absence of absorption. An absorbing sample gas in the cavity increases the rate of decay, thus indicating the presence of an absorbing species. The advantages of the method are high sensitivity and a small sample volume, while indirect measurement is an important drawback: as the measured parameter is the rate of light intensity decay, decay caused by absorption by the analyte of interest has to be distinguished from the one caused by the mirrors and other cavity-dependent losses.

In linear detection, sensitivity is limited by laser power fluctuations, and a considerable improvement can be obtained by the dark background methods, in which one measures a quantity that is directly proportional to absorption, rather than that part of the laser beam which is absorbed. In the visible, this can be done by monitoring the fluorescence from the upper level of the transition. In the IR, however, the spontaneous emission rate is too low, and most of the excess vibrational energy is converted to heat through inelastic collisions.

The fluorescence method requires that a certain part of the excitation should relax through radiative channels. This condition is fulfilled by detecting atoms and molecules in the UV, visible, and near-IR spectral regions. As a principal advantage of the fluorescence techniques, the observed signal is proportional to the concentration of the measured species and the accuracy, therefore, depends on the magnitude of the signal relative to detector noise. The sensitivity is so high, that it makes it possible to detect single atoms in the laser beam.

The basic principle of all photothermal (PT) techniques is the absorption of light in a sample leading to a change in its thermal state. This may be a change in temperature or another thermodynamic parameter of the sample that is related to temperature. Measurement of either the temperature, pressure or density change that occurs due to optical absorption is ultimately the basis for all PT spectroscopic methods. PT analysis can be considered as an indirect absorption measurement, since the measured quantity is not an optical signal. (It should be noted here that the classical absorption measurement is not a direct measurement either. Though the measured value in this case is an optical one, namely the transmitted light, the absorbed light quantity is derived from the difference of the incident energy and the transmitted one). The sample heating which produces the PT signal is directly correlated to the absorbed electromagnetic energy. Unlike in conventional transmission spectroscopy, neither scattered nor reflected light contributes to the signal. Although a PT effect can be induced by any light source, lasers are nowadays the preferred source of excitation for two reasons: (i) To a first approximation, the PT signal is proportional to the temperature rise in the sample and thus proportional to the absorbed energy. (ii) For many applications, the selectivity of a PT analysis, as with any other absorption method, depends on the tunability of the excitation wavelength.

PA spectroscopy is an indirect technique in that an effect of absorption is measured rather than absorption itself. Hence the name of photoacoustic: light absorption is detected through its accompanying acoustic effect. The advantage of photoacoustics is that the absorption of light is measured on a zero background; this is in contrast with direct absorption techniques, where a decrease of the source light intensity has to be observed. The spectral dependence of absorption makes it possible to determine the nature of the trace components. The PA method is primarily a calorimetric technique, which measures the precise number of absorbent molecules by simply measuring the amplitude of an acoustic signal. In LPAS the nonradiative relaxation which generates heat is of primary importance. In the IR spectral region, nonradiative relaxation is much faster than radiative decay.

PA spectroscopy relies on the PA effect for the detection of absorbing analytes. The sample gas is in a confined (resonant or nonresonant) chamber, where modulated (e.g., chopped) radiation enters via an IR-transparent window and is locally absorbed by IR-active molecular species. The temperature of the gas thereby increases, leading to a periodic expansion and contraction of the gas volume synchronous with the modulation frequency of the radiation. This generates a pressure wave that can be acoustically detected by a suitable sensor, e.g., by a microphone. The advantages of the PA method are high sensitivity and small sample volume; besides, the acoustic measurement makes optical detection unnecessary. The main drawback is caused by the sensitivity to acoustic noise, because the measurements are based on an acoustic signal. A comparison of the linear laser spectroscopy methods is presented in Table 1 (Zharov & Letokhov, 1986).

Method / Characteristics	Absorption	Fluorescence	PA
Spectral range	UV – far IR	UV and visible	UV – far IR
Sensitivity (cm^{-1})	10^{-5} – 10^{-9}	Up to single atoms	10^{-7} – 10^{-10}
Time resolution (s)	1	1 – 10^{-12}	1 – 10^{-3}
Necessary conditions	-	Radiative channels of relaxation	Nonradiative channels of relaxation

Table 1. Comparison of linear laser spectroscopy methods.

The favorable properties of LPAS are essentially determined by the characteristics of the laser. The kind and number of detectable substances are related to the spectral overlapping of the laser emission with the absorption bands of the trace gas molecules. Thus, the accessible wavelength range, tunability, and spectral resolution of the laser are of prime importance. With respect to minimum detectable concentrations (LPAS sensitivity), a laser with high output power P_L is a benefit, because the PA signal is proportional to P_L. The broad dynamic range is an inherent feature of LPAS and therefore is not affected by the choice of the radiation source. In contrast to remote-sensing methods, LPAS is a detection technique applied locally to samples enclosed in a PA cell. In order to still obtain some spatial resolution, either the samples have to be transported to the system, or the system has to be portable. The temporal resolution of LPAS is determined by the time needed for laser tuning and the gas exchange within the cell. Thus, a small volume PA cell and a fast tunable laser are a plus.

The availability of suitable laser sources plays a key role, as they control the sensitivity (laser power), selectivity (tuning range), and practicability (ease of use, size, cost, and reliability) that can be achieved with the photoacoustic technique. The CO_2 laser perfectly fits the bill for a trace gas monitoring system based on LPAS. This IR laser combines simple operation and high output powers. The frequency spacing between two adjacent CO_2-laser transitions range from 1 to 2 cm^{-1}. By contrast, the typical width of a molecular absorption line is approximately 0.05 to 0.1 cm^{-1} for atmospheric conditions. Since this is not a continuously tunable source, coincidences between laser transitions and trace gas absorption lines are mandatory. Fortunately, this does not hamper its applicability to trace gas detection, as numerous gases exhibit characteristic absorption bands within the wavelength range of the CO_2 laser which extends from 9 to 12 μm when different CO_2 isotopes are used. The CO_2 laser spectral output occurs in the wavelength region where a large number of compounds (including many industrial substances whose adverse health effects are a growing concern) possess strong characteristic absorption features and where absorptive interferences from water vapors, carbon dioxide, and other major atmospheric gaseous components may influence the measurements.

2.2 PA effect in gases

The PA effect in gases can be divided into five main steps (Fig. 1):

1. Modulation of the laser radiation (either in amplitude or frequency) at a wavelength that overlaps with a spectral feature of the target species; an electrooptical modulation

device may also be employed, or the laser beam is modulated directly by modulation of its power supply; the extremely narrowband emission of the laser allows the specific excitation of molecular states; the laser power should be modulated with a frequency in the range $\tau_{th} >> 1/f >> \tau_{nr}$, where τ_{th} is the thermal relaxation time, and τ_{nr} the nonradiative lifetime of the excited energy state of the molecule.

2. Excitation of a fraction of the ground-state molecular population of the target molecule by absorption of the incident laser radiation that is stored as vibrational-rotational energy; the amount of energy absorbed from the laser beam depends on the absorption coefficient, which is a function of pressure.
3. Energy exchange processes between vibrational levels (V-V: vibration to vibration transfer) and from vibrational states to rotational and translational degrees of freedom (V-R, T transfer); the energy which is absorbed by a vibrational-rotational transition is almost completely converted to the kinetic energy of the gas molecules by collisional de-excitation of the excited state; the efficiency of this conversion from deposited to translational energy depends on the pressure and internal energy level structure of the molecule; vibrational relaxation is usually so fast that it does not limit the sensitivity; however, notable anomalies occur in the case of diatomic molecules, such as CO, where vibrational relaxation is slow in the absence of a suitable collision partner, and of the dilute mixtures of CO_2 in N_2, where the vibrational energy is trapped in slowly relaxing vibrational states of N_2; the kinetic energy is then converted into periodic local heating at the modulation frequency.
4. Expansion and contraction of the gas in a closed volume that give rise to pressure variation which is an acoustic wave; the input of photon energy with correct timing leads to the formation of a standing acoustic wave in the resonator.
5. Monitoring the resulting acoustic waves with a microphone; the efficiency at which sound is transmitted to the microphone depends on the geometry of the cell and the thermodynamic properties of the buffer gas.

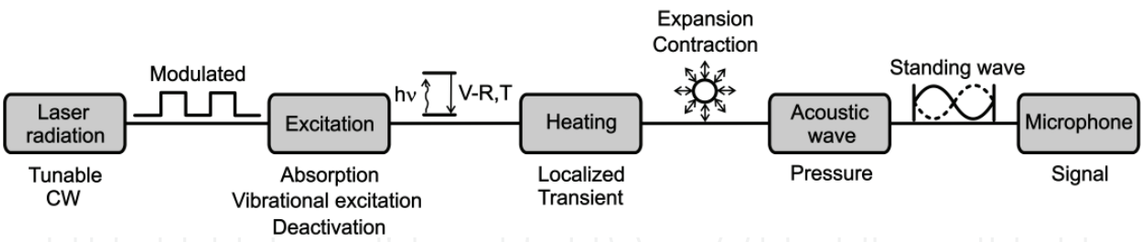


Fig. 1. Schematic of the physical processes occurring during optical excitation of molecules in photoacoustic spectroscopy.

From kinetic gas theory it can be estimated that a molecule performs 10^9-10^{10} collisions per second at 1 bar pressure. This means that at atmospheric pressure the photon energy is transformed into an acoustical signal in about 10^{-5}-10^{-6} s. For most polyatomic molecules signal production is even faster. The time needed by the pressure wave to travel from the laser beam area to the microphone in the acoustic cell is therefore in most cases longer than the vibrational relaxation time. For a distance of a few centimeters this transit time is about 10^{-4} s. The time delay between excitation and detection of the pressure wave, however, is influenced not only by energy transfer processes and the transit time, but also by the response time of the gas-microphone system, being about 10^{-4} s or longer (Hess, 1983).

2.3 Typical laser photoacoustic setup

A typical setup of a resonant LPAS, as used in the authors' laboratory for gas studies, is shown in Fig. 2. The continuous wave laser radiation is amplitude-modulated by a mechanical chopper operating at an acoustic resonance frequency of the PA cell. It is then focused by a lens and directed through the resonant PA cell. The transmitted laser power is monitored with a powermeter (signal P_L in Fig. 2). Inside the cell the radiation produces pressure modulation recorded by microphone as an acoustical signal V, which is processed by a lock-in amplifier locked to the chopper frequency. The normalized absorption can then be deduced as being proportional to V/P_L ratio (Cristescu et al., 1997, Dumitras et al., 2007a).

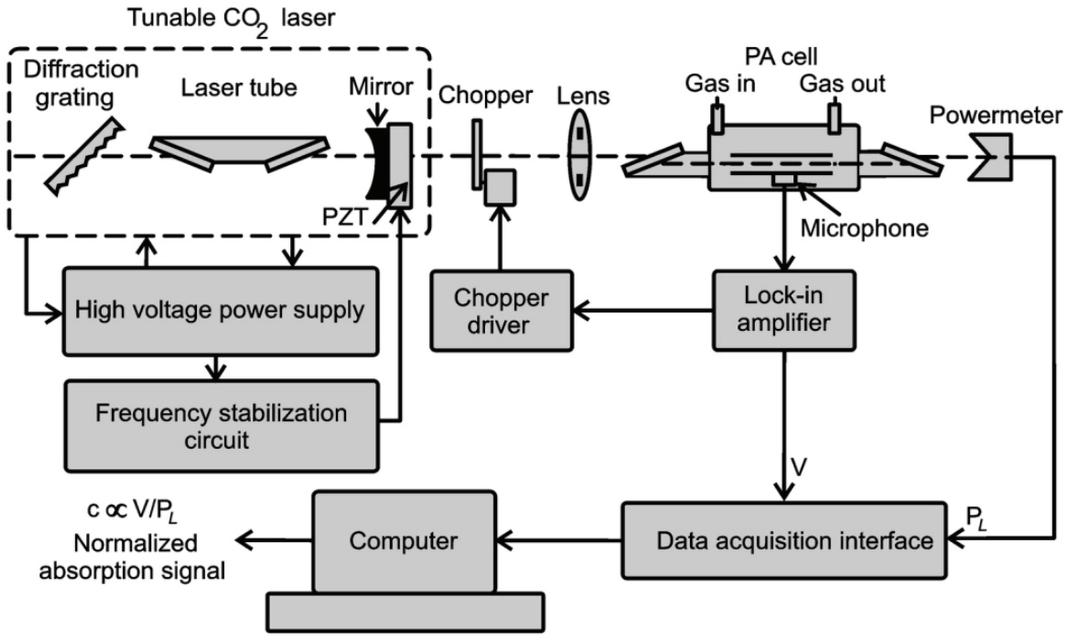


Fig. 2. Typical laser photoacoustic setup for trace gas measurements.

The power reading after beam passage through the PA cell can only be used for "transparent" gas samples. Let us evaluate if this condition is fulfilled. If the absorption is assumed to follow the Beer-Lambert law (Eq. 1), in the case of small absorption, the fractional absorption of the laser beam in the PA cell is given as $\Delta P/P(0) \cong \alpha Lc$ (Eq. 2). The quantity αLc is known as the optical density of the gas in the resonator tube (this quantity is also called absorbance). Therefore, the PA signal proportional to ΔP depends linearly on the absorption coefficient, and its dependence on gas concentration is also linear. At $\alpha Lc = 0.06$, a deviation of ~3% results from the linear behavior (~10% for $\alpha Lc = 0.07$). An optical density of 0.06 (an ethylene concentration of 65 ppmV for $L = 30$ cm, the length of our cell) may thus be regarded as the upper limit of the linear range of a PA detector. Consequently, the PA signal can be modeled as a linear function of concentration in the full range from a few tens of pptV to 65 ppmV ethylene, so that the range spans over 6 orders of magnitude! Taking into account typical values for the absorption coefficients of the species to be measured (e.g., for ethylene at concentrations in the range 1 ppbV-10 ppmV, $\alpha c \cong 3\text{x}10^{-8}\text{-}3\text{x}10^{-4}$ cm^{-1}) and

usual lengths of the PA cells (~30 cm), the fractional absorption is very small (10^{-6}-10^{-2}), which means that in the worst case less than 1% of the incident laser power is absorbed in the sample gas inside the PA cell. It follows that the powermeter measures the real value of the laser power inside the PA cell (we have "transparent" gases).

Another advantage of photoacoustic spectroscopy as a tool for trace gas analysis is that very few photons are absorbed as the laser beam passes through the sample cell. As a result, notwithstanding the losses from absorption in the windows, the transmitted beam typically has sufficient power for analyzing samples in successive cells, via a multiplexing arrangement. A multiplexed photoacoustic sensor can be used to monitor many different samples simultaneously so that one instrument can be deployed to monitor up to 20 different locations within a clean room, industrial plant or other facility (Pushkarsky et al., 2002).

Following the terminology introduced by Miklos et al. (Miklos et al., 2001), the name 'PA resonator' will be used for the cavity in which the resonant amplification of the PA signal takes place. The term PA cell (or PA detector; both terms are used in the literature to describe the device in which the PA signal is generated and monitored) is reserved for the entire acoustic unit, including the resonator, acoustic baffles and filters, windows, gas inlets and outlets, and microphone(s). Finally, PA instrument (PA sensor) stands for a complete setup, including the PA cell, light source, gas handling system, and electronics used for signal processing.

It is interesting to mention that the *reverse* PA effect, called "sonoluminiscence", consists in the generation of optical radiation by acoustic waves, while the *inverse* PA effect is the generation of sound due to optical energy being lost from a sample, instead of being deposited in a sample as in the usual PA effect (Tam, 1986).

3. Photoacoustic signal

3.1 Resonant cells

A PA cell can be operated either in nonresonant mode or at an acoustic resonance frequency specific to the PA resonator. In the so-called nonresonant mode, the modulation frequency is much lower than the first acoustic resonance frequency of the PA resonator. In this case, the wavelength of the generated acoustic wave is larger than the cell dimensions. Thus, the generation of standing acoustic waves is not possible. A nonresonant PA cell lacks any means of energy accumulation in the acoustic wave, i.e., the induced pressure fluctuations are a function of the energy absorbed on that cycle alone and, in fact, any acoustic energy remaining from previous cycles tends only to produce noise on the desired signal. The main drawbacks of the nonresonant scheme are the low modulation frequency, which makes the system susceptible to $1/f$ noise, and the relatively large background signal generated by absorption in the windows of the cell and by radiation scattered to the walls. Nevertheless, the acoustically nonresonant cell has an advantage in low-pressure operation, as the signal, and hence the SNR, remains constant as pressure is decreased, whereas for the resonant cell, it drops almost linearly with decreasing pressure (Fig. 3) (Dumitras et al., 2007b). Also, the background signal, which limits the sensitivity of the nonresonant cell at atmospheric pressure, has been found to depend approximately linearly on pressure and would be less troublesome in low-pressure operation (Gerlach & Amer, 1978).

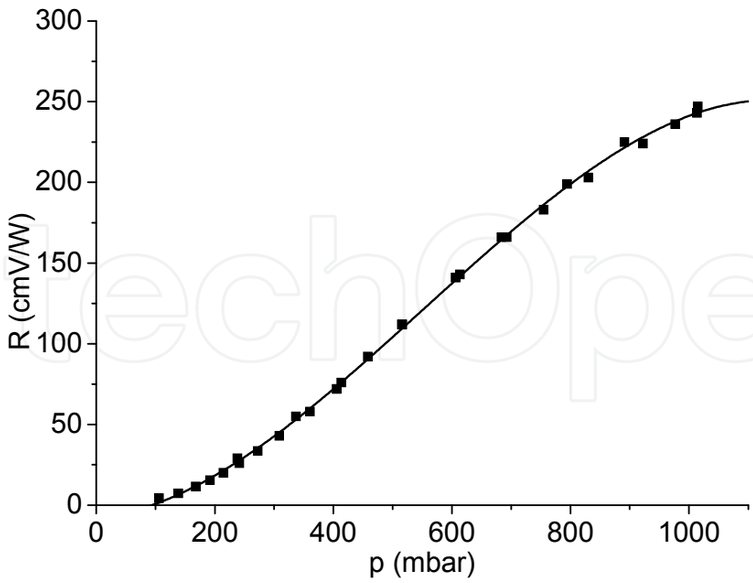


Fig. 3. Dependence of the PA cell responsivity on the total gas pressure in the cell (measured with 1 ppmV ethylene in nitrogen).

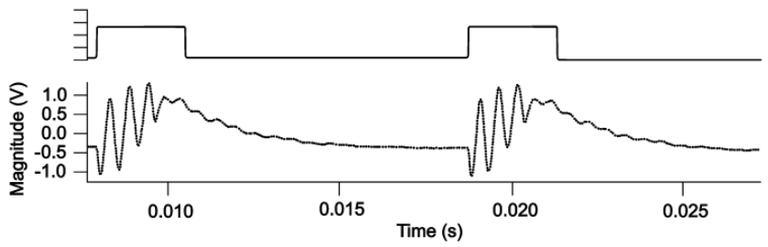
Nonresonant operation can compete with enhanced resonant operation only at much lower frequencies and smaller cell volumes; however, a number of practical difficulties have been cited. At low frequencies, gas inlet-outlet ports act as pneumatic short circuits for the induced pressure (Kritchman et al., 1978). Excess acoustic energy in previous cycles of the modulated light can produce noise in the nonresonant signal, while in resonant operation this type of noise is avoided because the energy in each cycle contributes to a standing wave (Kamm, 1976). For the small, nonresonant cell, attachment of the microphone can lead to difficulties in extracting the optimum pressure response signal (Dewey, 1977).

With increasing modulation frequency, the acoustic wavelength equals the cell dimensions at a certain point, and the resonant modes of the cell can be excited, leading to an amplification of the signal. The signal can be boosted manifold by: a) designing the sample cell as an acoustic resonance chamber, so that the pressure fluctuations produced by spatially and temporally nonuniform excitation contribute to standing acoustic waves within the chamber, and b) minimizing dissipation of the acoustic energy and modulating the laser beam spatially and temporally at a frequency which coincides with one of the natural resonant acoustic frequencies of the chamber. The system becomes an acoustic amplifier in the sense that the energy existing in the standing wave is many times higher than the energy input per cycle, and the signal is amplified by a quality factor *Q*. The final signal amplification obtainable depends on the resonator losses. After an initial transient state, during which energy is accumulated in the standing acoustic wave, a steady state is reached in which the energy lost per cycle by various dissipation processes is equal to the energy gained per cycle by absorption of IR laser photons. Resonance properties mainly depend on the geometry and size of the cavity. For an acoustically resonant PA cell, important parameters will include gas characteristics such as heat capacity, thermal conductivity, viscosity, energies and relaxation times of the molecular vibrations and the sound velocity which determines the resonant frequencies of the cavity. Other parameters

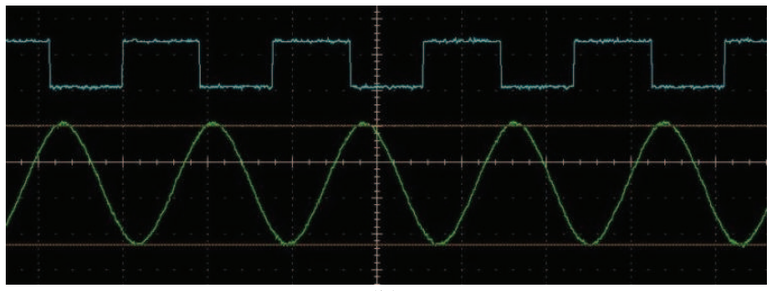
govern the loss mechanisms that determine the quality factors of the resonances and also cause small shifts in the resonant frequencies.

A comparison of the microphone signals for nonresonant operation at 100 Hz and resonant operation at 564 Hz is depicted in Fig. 4 (a) and (b), respectively, together with the chopper waveforms. For nonresonant operation, the laser beam was amplitude-modulated with a duty cycle (pulse duration divided by the pulse period) of 25%, and the PA signal exhibits ringing at the resonant frequency on top of the 100-Hz square wave. For resonant operation, the laser beam was amplitude-modulated with a duty cycle of 50% and the microphone output was simply a coherent sine wave. In Fig. 4 (b), the data were recorded with a concentration of 1 ppmV of ethylene in the PA cell.

The resonant cells can be adequatelly characterized by a model based on an acoustic transmission line (Cristescu et al., 2000).



(a)



(b)

Fig. 4. Microphone signals for: (a) nonresonant operation of the PA cell (Pushkarsky et al., 2002); (b) resonant operation of the PA cell (our cell), recorded with a Tektronix DPO 7104 Digital Oscilloscope, horizontal scale 1 ms/div, vertical scales 1 V/div. (rectangle wave) and 0.5 V/div. (sine wave amplified x 100).

3.2 Resonance frequencies

Several distinct resonances can be generated if the dimensions of a cavity are comparable with the acoustic wavelength. The standing wave patterns and resonance frequencies depend on the shape and size of the PA resonator. The most frequently used resonator is the cylinder, the symmetry of which coincides well with that of a laser beam propagating along the cylinder axis. The natural acoustic resonance frequencies of a lossless cylindrical resonator (fully reflecting walls) are determined as a solution of the wave equation in cylindrical coordinates (Hess, 1983):

$$f_{kmn} = \frac{v_s}{2}\left[\left(\frac{k}{L}\right)^2 + \left(\frac{\alpha_{mn}}{\pi r}\right)^2\right]^{1/2}, \tag{3}$$

where v_s is the sound velocity, L and r are the length and radius of the cylinder, the k, m, n indices (non-negative integers) refer to the values of the longitudinal, azimuthal, and radial modes, respectively, and α_{mn} is the n-th root of the derivative of the m-th Bessel function:

$$\frac{\mathrm{d}J_m(z)}{\mathrm{d}z} = 0 \tag{4}$$

($\alpha_{00} = 0$, $\alpha_{01} = 3.8317$, $\alpha_{02} = 7.0153$, $\alpha_{10} = 1.8412$, $\alpha_{11} = 5.3311$, $\alpha_{12} = 8.5360$, etc.). For the first longitudinal mode, $k = 1$, $m = 0$, $n = 0$ and $f_{100} = f_0 = v_s/2L$.

In deducing Eq. (3), it was assumed that there was no phase shift on reflection of the pressure wave from the cavity walls caused either by wall compliance or boundary layer effects. If we depart from the assumption of complete wall rigidity, the boundary layer can be seen to cause significant frequency deviations from the above formula. To evaluate the frequency from Eq. (3), we must know the sound velocity, which may vary with frequency and pressure due to molecular relaxation effects and the nonideal behavior of the gas.

In reality, frequencies at the resonances are somewhat smaller. The corresponding resonance frequencies for PA resonators with open-open ends can be obtained from the following expression (Morse & Ingard, 1986):

$$f_0 = \frac{v_s}{2(L + \Delta L)}, \tag{5}$$

where the quantity ΔL is the so-called end correction, which should be added to the length of the pipe for each open end. Physically, the end correction can be understood as an effect of the mismatch between the one-dimensional acoustic field inside the pipe and the three-dimensional field outside that is radiated by the open end. The end correction can be approximated by the following expression: $\Delta L \cong 0.6r$, where r is the radius of the pipe (Miklos et al., 2001). More precisely, the end correction slightly decreases with frequency; therefore the resonance frequencies of an open pipe are not harmonically related but slightly stretched. In our experimental setup, the resonance frequency for 0.96 ppmV of ethylene in pure nitrogen is 564 Hz at L = 30 cm. By taking v_s = 343 m/s in nitrogen at 22°C (the sound velocity in nitrogen of 330 m/s at 0°C was corrected for the room temperature), we have $\Delta L \cong 0.2$ cm for the two open ends of our PA resonator and $\Delta L \cong 0.6r$ (r = 0.35 cm).

In an ideal gas, the sound velocity is given by:

$$v_s = (\gamma RT / M)^{1/2}, \tag{6}$$

where $\gamma = C_p/C_v$ is the ratio of specific heats at constant pressure and volume, R is the ideal-gas constant, T is the absolute temperature, and M is the molecular weight. The sound velocity in an ideal gas only depends on temperature and remains unchanged at pressure modifications if $\gamma$is constant. In the case of ideal gases, γ= 1.4 for diatomic gases and γ= 1.33 for triatomic gases. Experimentally, the following values have been measured: 1.404 for N_2, 1.401 for O_2, 1.404 for CO, 1.32 for H_2O, 1.31 for NH_3, 1.31 for CH_4, and 1.25 for C_2H_4.

For nonideal gases, the sound velocity can be approximately calculated by the following formula:

$$v_s = \left[\gamma\left(RT + 2Bp\right) / M\right]^{1/2}, \tag{7}$$

where B is the second virial coefficient and p is the pressure.

Little attention has been given to the role of the buffer gas (defined as the optically nonabsorbing gaseous component in photoacoustic detectors). In principle, the molecular weight and the thermodynamic and transport properties of the buffer gas should have a significant impact on the photoacoustic signal. One would also expect the energy transfer between the absorbing species and the buffer gas to play an important role in PA detection (Thomas III et al., 1978; Gondal, 1997). In a mixture of ideal gases, the sound velocity $\overline{v}_s$ and consequently the resonant frequencies of a PA resonator depend on the effective specific heat ratio and the average mass of the mixture:

$$\overline{v}_s = \left(\overline{\gamma} RT / \overline{M}\right)^{1/2}, \tag{8}$$

where the specific heat ratio $\overline{\gamma}$ and the average molecular weight $\overline{M}$ are:

$$\overline{\gamma} = \frac{xC_p^b + \left(1-x\right)C_p^a}{xC_v^b + \left(1-x\right)C_v^a}, \tag{9}$$

$$\overline{M} = xM^b + \left(1-x\right)M^a. \tag{10}$$

Here C_p^b, C_v^b, C_p^a and C_v^a are the heat capacities of the buffer and absorbing gases, respectively; M^b and M^a are their molecular weights; and x is the fractional concentration of the buffer gas. When the molecular weight of the buffer gas is increased, the resonance frequency of the PA resonator shifts to lower values. In conclusion, the resonance frequency is a sensitive function of temperature and gas composition, both of which influence the speed of sound.

At a fixed temperature, v_s also depends on the water content in the air (Rooth et al., 1990):

$$v_s = v_{s0}^{'}\left[1 - \frac{p_w}{p_{air}}\left(\frac{\gamma_w}{\gamma_{air}} - \frac{5}{8}\right)\right]. \tag{11}$$

Here γ_w and γ_{air} are the ratios of the specific heats of water vapor and air. The partial pressures of water and air are denoted as p_w and p_{air}. The sound velocity in dry air is written as $v_{s0}^{'}$. The increase of the resonance frequency of a 30-cm long longitudinal resonator at ambient temperature is 0.90 Hz for 1% of water vapors added to the gas. For all practical purposes, the variation of the resonance frequency with the CO_2 concentration is negligible: -0.15 Hz per 1000 ppmV. For a given water vapor concentration, the resonance frequency provides information about the gas temperature inside the resonator. In most cases, the PA cell resonance frequency has to be determined experimentally.

Since the resonance frequency is proportional to the sound velocity, the temperature dependence of the sound velocity is directly mirrored by the resonance frequency. The sound velocity in air has a temperature coefficient of about 0.18%/°C, thus a frequency shift $\delta f \cong 0.0018 f_0 \Delta T$ is expected for a temperature change ΔT (°C) (Miklos et al., 2001). The true resonance frequency may therefore deviate from the fixed modulation frequency by δf. Then the PA signal will not be excited at the peak of the resonance, but slightly to one side. Since a detuning from the resonance peak by 0.46 ($\Delta f(10\%)/\Delta f(\mathrm{FWHM}) = 16/35$) results in a 10% drop of the PA signal (see Fig. 5), the detuning should be smaller than $\pm 0.23 f_0/Q$ for 10% signal stability. This stability can be ensured, if the condition $Q\Delta T \leq 128$ ($\delta f \leq 0.23\Delta f$ or $0{,}0018 f_0 \Delta T \leq 0.23\Delta f$ or $Q\Delta T \leq 0.23/0.0018$) is fulfilled ($\Delta T \leq 7.9$°C in our case for Q =16.1). The corresponding condition for PA signal stability of 2% can be written as $Q\Delta T \leq 64$ ($\Delta T \leq 4$°C in our case). These examples clearly show that low-Q photoacoustic resonators are not sensitive to temperature variations and consequently do not need temperature stabilization or active tracking of the resonance to adjust the modulation frequency.

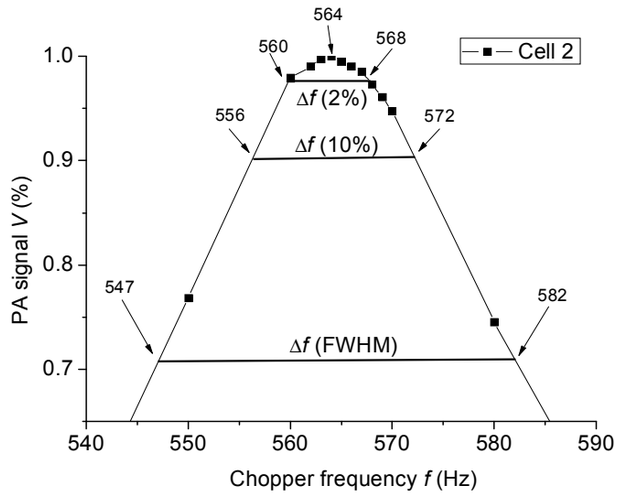


Fig. 5. Resonance curve of our PA cell showing the full width at half maximum (FWHM) and the full widths for a signal drop of 2% and 10% from its maximum.

3.3 Dissipation processes

The various dissipation processes occurring in an acoustic cavity were first discussed at length by Kamm (Kamm, 1976). The energy accumulation attainable in a standing wave of a resonant cavity is many times larger than the energy loss occurring during a single period of an acoustic oscillation. This acoustical amplification effect is limited, however, by various dissipation processes. The losses can be divided into surface effects and volumetric ones (Johnson et al., 1982). The surface losses are due to the interaction of the standing wave with the internal resonator surface and may be subdivided into the following dissipation processes:

1. compliance of the chamber walls;
2. dissipation at the microphone diaphragm;
3. losses due to wave scattering at surface obstructions such as gas inlet/outlet, microphones, and windows;
4. viscous and thermal dissipation in the boundary layer at the smooth internal surfaces.

In a carefully designed high quality resonator, the contribution of the first three effects can be minimized. The dominant contribution is caused by the viscous and thermal boundary layer losses. Throughout the major portion of the resonator volume the expansion and contraction of the gas occur adiabatically. We neglect heat conduction and viscous losses in the volume of the gas because the acoustic power loss from these effects is very small. However, the wall consists of a material with a thermal conduction coefficient much greater than that of the gas. Thermal dissipation occurs because expansion and contraction of the gas do not proceed adiabatically near the walls, where the process will change to isothermal. The temperature variation changes exponentially from the adiabatic propagation regime in the gas to a zero value at the wall. This leads to heat conduction within a transition region (thermal boundary layer), which is responsible for the thermal dissipation process. Outside a thin boundary layer with thickness d_h, near the wall, the thermal losses can be neglected:

$$d_h = \left(\frac{2K}{\rho \omega C_p} \right)^{1/2} . \tag{12}$$

Here K is the thermal conductivity of the gas, ρ is the density of mass, C_p is the molar heat capacity, and $\omega = 2\pi f$ is the angular frequency.

The viscous dissipation can be explained by the boundary conditions imposed by the walls. At the surface, the tangential component of the acoustic velocity is zero, whereas inside the cavity, it is proportional to the acoustic pressure gradient. Thus, viscoelastic dissipation occurs in a transition region with a thickness d_v, which is called the viscous boundary layer:

$$d_v = \left(\frac{2\mu}{\rho \omega} \right)^{1/2} , \tag{13}$$

where μ is the viscosity coefficient.

Equations (12) and (13) are only valid if d_h and d_v are much smaller than the radius of the PA resonator (d_h, $d_v << r$), which yields a lower frequency limit. The upper frequency limit is reached when the wavelength of sound is comparable to the cross-sectional dimensions of the tube ($\lambda_s = v_s/f_0 \cong r$). The magnitude of d_h and d_v can be calculated by using the properties of nitrogen at standard pressure (p = 1 atm) and room temperature: $K = 2.552 \times 10^{-2}$ W/(m K), $\mu = 1.76 \times 10^{-5}$ Pa s, $C_p = 1.04 \times 10^3$ J/(kg K), $\rho = 1.142$ kg/m^3 and $\gamma = C_p/C_v = 1.4$. As a result, the values for the thermal and viscous boundary layer thicknesses are, respectively: $d_h = (2K/\rho\omega_0 C_p)^{1/2} = 2.6(f_0)^{-1/2}$ (mm Hz$^{1/2}$) $\cong$ 0.110 mm (at f_0 = 564 Hz) and $d_v = (2\mu/\rho\omega_0)^{1/2} = 2.2(f_0)^{-1/2}$ (mm Hz$^{1/2}$) $\cong$ 0.093 mm (at f_0 = 564 Hz). Therefore, at atmospheric pressure and audio frequencies, both boundary layers are only a fraction of a millimeter thick.

The volumetric or bulk losses are caused by processes that tend to establish equilibrium in the propagating wave. These damping processes are:

1. free space viscous and thermal dissipation;
2. diffusion effects;
3. radiation effects; and
4. relaxational damping (dissipative relaxation processes within polyatomic gases).

Friction due to compressional motion and the transformation of organized energy into heat due to temperature gradients are responsible for the free space viscous and thermal losses.

These two processes are often called Stokes-Kirchhoff losses and are small compared with surface damping. Diffusion and radiation effects are normally very small. Nevertheless, radiation losses through openings, e.g., pipes connecting the resonator to buffer volumes, cannot be neglected. The radiation losses can be reduced by increasing the acoustic input impedance of the openings. This is achieved by terminating the cavity resonator at the openings with acoustic band-stop filters, which prevent sound escape from the resonator. Relaxational effects can add a significant contribution in diatomic and polyatomic molecules. The reason for the relaxational losses is the phase difference between gas pressure and density in the dispersion region, leading to an irreversible conversion of sound energy into thermal energy.

3.4 Quality factor

The amount of signal enhancement that occurs when the laser is modulated at a resonance frequency is determined by the quality factor. At resonance, the amplitude of the PA signal is Q times larger than the amplitude far from the resonance frequency, i.e., the amplification is equal to the value of the Q factor. The quality factor of the system, Q, is the ratio between the energy stored in a specific mode (the acoustic wave) and the energy losses per cycle of this acoustic wave:

$$Q = \frac{2\pi \text{ accumulated energy}}{\text{energy lost over one period}}. \tag{14}$$

For high Q values the quality factor can be deduced dividing the resonance frequency by its bandwidth at the 0.707 amplitude point:

$$Q = \frac{f_0}{\Delta f} = \frac{\omega_0}{\Delta\omega}, \tag{15}$$

where f_0 and Δf are the resonance frequency and the full-width value of the resonance profile ($\omega_0 = 2\pi f_0$ and $\Delta\omega = 2\pi\Delta f$). The full width is measured between the points where the amplitude of the resonance profile is at $1/\sqrt{2}$ the peak value amplitude (half-maximum values of the intensity). Therefore, Δf is also called the full width at half maximum (FWHM). Q is typically between 10 and 50 for longitudinal resonators, but can be as high as 1000 for spherical cavities.

Also, the quality factor can be calculated as (Kamm, 1976; Bernegger & Sigrist, 1987):

$$Q = \frac{2S}{2\pi r\left[d_v + (\gamma - 1)d_h\right]}, \tag{16}$$

where S stands for the cross section of the resonator tube and r for the radius of the tube. By introducing the radius (r = 3.5 mm) of the PA resonator we used and the values for the thermal and viscous boundary layer thicknesses determined in the previous section, Eq. (16) yields Q = 14.2, in agreement with the experimentally determined value (Q = 16.1).

The overall Q factor for a resonance may be found by summing all the losses, expressed as $1/Q_i$:

$$\frac{1}{Q_{tot}} = \sum_i \frac{1}{Q_i}, \tag{17}$$

In practice, we only include three contributions: viscous and thermal dissipation in the boundary layer at the smooth internal surfaces (surface loss), free space viscous and thermal dissipation, and relaxation losses (volumetric losses).

3.5 Pressure amplitude

The transformation of the absorbed laser energy into heat is usually modeled by a simple relaxation process, while the well-known acoustic-wave equation is applied to calculate the sound-pressure field. The laws of fluid mechanics and thermodynamics can be used to model the acoustic and thermal wave generation in gases. The governing physical equations are the laws of conservation of energy, momentum, mass, and the thermodynamic equation of state. The physical quantities characterizing the acoustic and thermal processes are the temperature T, pressure p, density ρ, and the three components of the particle velocity vector $\mathbf{v}$. By eliminating the variables T, ρ, and $\mathbf{v}$ (and by neglecting the influence of the thermal and viscous interactions of the gas), a linear (inhomogeneous) wave equation can be derived for the acoustic pressure changes, p (Miklos et al., 2001):

$$\frac{\partial^2 p(\mathbf{r},t)}{\partial t^2} - v_s^2 \nabla^2 p(\mathbf{r},t) = (\gamma - 1)\frac{\partial H(\mathbf{r},t)}{\partial t}, \tag{18}$$

where $H(\mathbf{r},t)$ is the heat density deposited in the gas by light absorption. The term on the right-hand side of the equation describes the heat input changes over time. When the heat input is constant, this term is zero and no pressure wave is generated. Thus, the heat input must be modulated, which requires that the laser radiation be also amplitude or frequency modulated. A modulated laser beam generates periodic sound due to the periodic localized heating of the gas. From an acoustic point of view, the PA cell is a linear acoustic system, which responds as a whole to the disturbance generated by light absorption. The differential equation (18) is not valid for capillary tubes with a small diameter ($2r \approx d_v$, d_h) nor for gases with exceptionally high viscosity or heat conductivity.

When the absorbing gas can be modeled by a two-level system consisting of the vibrational ground and the excited state, Meyer and Sigrist (Meyer & Sigrist, 1990) found that the amplitude of heat production rate, H, is given by:

$$H(\mathbf{r},t) = \alpha_p I(\mathbf{r},t), \tag{19}$$

where $I(\mathbf{r},t)$ is the intensity of the laser beam. This equation is valid only when the laser beam is slowly chopped in the kHz range or below, and in the absence of optical saturation.

If the cross-sectional dimensions of a resonator are much smaller than the acoustic wavelength, the excited sound field develops a spatial variation only along the length of the resonator, i.e., a one-dimensional acoustic field is generated. A narrow pipe (or tube) can be regarded as a one-dimensional acoustic resonator. A pressure wave propagating in the pipe will be reflected by an open end with the opposite phase. Through multiple reflections a standing wave pattern with pressure nodes will be formed. Therefore, open pipes should have resonances when the pipe length is equal to an integer multiple of the half wavelength.

Bernegger and Sigrist (Bernegger & Sigrist, 1987) proved that the plane acoustic wave propagation can be modeled by the one-dimensional analogue of the electrical current flow

in a transmission line. According to this theory, a cell constant C (Pa cm/W) only dependent on the geometry of the cell (it includes the losses of the PA resonator), which relates the pressure amplitude p with the absorbed laser power P_L, can be defined at resonance frequency:

$$p = C(\omega = \omega_0)\alpha_p P_L , \tag{20}$$

where p (N/m² = Pa) is the pressure response of the cell, α_p (cm^{-1}) is the absorption coefficient at a given pressure of the gas at the laser wavelength, and P_L (W) is the laser power. The units of C are given in Pa cm/W based on the usual dimensions of p, α_p, and P_L. Here, the angular frequency is $\omega_0 = 2\pi f_0$, where f_0 is the resonance frequency; for a longitudinal resonant cell, the first resonance frequency is $f_0 = v_s/2L$ (Eq. 3), so that $\omega_0 = \pi v_s/L$. C is usually determined by calibration measurements, where one single absorbing substance with known absorption spectrum is investigated.

Equation (20) implies that for a reasonably small laser power (no saturation), slow modulation frequency ω_0 ($\omega_0\tau << 1$, where τ is the thermal relaxation time characteristic for the cooling of the gas to equilibrium), and small absorption ($\alpha_p L << 1$), the sound pressure amplitude depends linearly on the absorption coefficient and the laser power.

3.6 Cell constant

For a given PA cell geometry ("high-Q" case), Kreuzer (Kreuzer, 1977) deduced that:

$$C(\omega_0) = \frac{(\gamma - 1)LQG}{\omega_0 V} , \tag{21}$$

where V is the volume of the PA resonator and G a geometrical factor (depending on the transverse beam profile but not on the cell length) on the order of 1 Pa m³/W s (Bijnen et al. (Bijnen et al., 1996) found a value G = 1.2 Pa m³/W s for their specific experimental conditions). Since the quantities in Eq. (21) are independent of the laser power and absorption coefficient, these factors can be regarded as characteristic setup quantities for PA resonators. The quantity C describes the sensitivity of the PA resonator at a given resonance frequency. It is widely known as the 'cell constant'. It depends on the size of the resonator, the frequency, and the Q factor of the resonance selected for PA detection. It also depends on the spatial overlap of the laser beam and the standing acoustic wave pattern. Its 'cell constant' name is therefore misleading, as it characterizes the complete measurement arrangement (including the acoustic resonator with a selected resonance, microphone position, and laser beam profile with spatial location) rather than the mere PA cell. Moreover, it depends on frequency, and its value differs for different resonance modes. Therefore, it would more appropriately be called a 'PA setup constant' (Miklos et al., 2001) rather than a 'cell constant'. However, since the name 'cell constant' is already established in the literature, we will continue to use it hereinafter.

As the cell constant is inversely proportional to an effective cross section defined by $S_{eff} = V/L$ and $\omega_0/Q = \Delta\omega$ (Eq. 15), it follows that:

$$C(\omega_0) = \frac{(\gamma - 1)G}{\Delta\omega S_{eff}} . \tag{22}$$

Based on this formula, we can estimate the magnitude of the cell constant. By introducing in Eq. (21) or Eq. (22) the values for our medium-Q resonator (r = 3.5 mm, L = 30 cm, Q = 16.1 and f_0 = 564 Hz; $S_{eff} \cong$ 0.4 cm², Δf = 35 Hz), it follows C = 4720 Pa cm/W, which is almost twice as much as the experimentally measured value (2500 Pa cm/W). If an open resonator is built into a closed PA cell, then the pressure generated by the PA effect will be distributed over the entire closed volume. Therefore, the total volume of the PA cell must be taken into account instead of the volume of the resonator. A PA resonator optimized for high-Q performance (S_{eff} ~80 cm², Q ~1000 at f_0 = 1 kHz) has a cell constant of about 800 Pa cm/W. The cell constant of a low-Q resonator is a complicated function of several parameters, and therefore cannot be determined with sufficient accuracy by calculation. It has to be determined experimentally by calibration measurements using certified gas mixtures.

The possibilities for improving the cell constant of acoustic resonators are limited (Miklos et al., 2001). The only parameter that can really be changed over a broader range is the effective cross section of the cell. A reduction of the cell diameter will increase the cell constant. A lower limit is set by the diameter and divergence of the laser beam employed. The cell constant for modulated measurements is inversely proportional to the FWHM value of the resonance profile. Unfortunately, the half width cannot be reduced indefinitely, because it scales approximately with the surface-to-volume ratio of the resonator. As the cross section of the cell is reduced, the surface-to-volume ratio increases. It is therefore impossible to achieve small cross sections and a small bandwidth (high Q) simultaneously. The smallest diameter used in practical systems is several millimeters, the largest about 10 cm.

Combining Eqs. (20) and (21), we have:

$$p = \frac{(\gamma - 1)\alpha_p L P_L Q G}{\omega_0 V}. \tag{23}$$

It should be noted that the amplitude of the PA pressure signal is a function of (1) the heat capacity of the mixture (γ), (2) laser power (P_L), (3) modulation frequency (ω_0), (4) vibrational relaxation times of the absorbing gas, and (5) damping effects of the buffer gas (Q). The first four factors contribute to the power going into the sound wave, and the last mechanism determines the Q of the resonances. From Eq. (23) it follows that the amplitude of the pressure wave (the PA pressure signal) is proportional to the absorption coefficient and laser power, but inversely proportional to the modulation frequency and effective cross section V/L of the PA resonator. Thus, the signal increases with decreasing resonator dimensions and modulation frequency. As the noise increases with a decrease of these parameters, there is a maximum in the SNR for a certain combination of cell size and modulation frequency.

For resonant operation, the modulation frequency is tuned to one of the resonance modes of the PA resonator, i.e., $\omega = \omega_m$. Not only the m-th mode, but all the other modes of the acoustic resonator are excited as a result. The resonance amplitude is proportional to Q, while the amplitudes of the other resonances are inversely proportional to the quantity $\omega^2 - \omega_m^2$. Therefore, distant resonances will not be excited efficiently. Certain resonances can be suppressed for special symmetry conditions, e.g., azimuthal modes cannot be excited if the cylindrical laser beam propagates exactly along the cylinder axis.

The measured PA signal also depends on the exact position of the microphone in the resonator. The signal detected by the microphone is proportional to the integral average of

the pressure over the microphone membrane. Since mostly miniature microphones are applied in photoacoustics, the integral can be approximated by the value of the pressure amplitude at the microphone location.

Angeli et al. (Angeli et al., 1992) reported a dependency of the cell constant on the kind of calibration gas. They concluded that the cell constant could not be determined unambiguously by a calibration measurement using a single absorbing species, indicating the "nonabsolute" character of photoacoustic spectroscopy. This result would have severe implications and would render analyses of multicomponent gas mixtures very difficult or impossible. Fortunately, Thöny and Sigrist (Thöny & Sigrist, 1995) proved that detailed investigations including a number of different gases and measurements on numerous laser transitions contradict those observations and revealed the expected independence of the cell constant within the measurement errors.

3.7 Optimization of the PA cell geometry

Since the PA signal is inversely proportional to the cell volume and modulation frequency, high PA signal levels can be obtained by taking a small cell volume (< 10 cm^3) and low modulation frequencies (< 100 Hz). However, noise sources (intrinsic noise of the microphone, amplifier noise, external acoustic noise) show a characteristic $1/f$ frequency dependence, and therefore the SNR of such a gas-microphone cell is usually quite small. The SNR of a PA cell can be increased by applying higher modulation frequencies (in the kHz region) and acoustic amplification of the PA signal. For this reason, resonant PA cells operating on longitudinal, azimuthal, radial, or Helmholtz resonances have been developed. Furthermore, resonant cells can be designed for multipass or intracavity operation.

A qualitative behavior for Q and ω_0 can be derived from simple geometrical considerations. So, for Q, the energy stored in a specific mode is proportional to the cell volume ($\propto r^2L$), while the energy losses per cycle of the acoustic wave are proportional to the cell surface ($2\pi rL$) and to the thicknesses $d_h \approx d_\nu = d \propto \omega_0^{-1/2} \propto L^{1/2}$. Therefore:

$$\omega_0 \propto L^{-1}, \tag{24}$$

$$Q(\omega_0) \propto (r^2L/rLL^{1/2}) \propto rL^{-1/2}, \tag{25}$$

and

$$C(\omega_0) \propto (L)(rL^{-1/2})/(L^{-1})(r^2L) \propto r^{-1}L^{1/2}. \tag{26}$$

which is represented graphically in Fig. 6. These equations show that the product $Q(\omega_0)C(\omega_0)$ is nearly independent of the cell dimensions for any kind of resonant PA cell. The operation of the cell in a longitudinal mode is more advantageous because it makes it possible to optimize the resonance frequency and the Q-factor independently, which cannot be achieved in the case of radial resonance.

Cell geometries with large diameter-to-length ratios designed to excite the resonance in the radial or azimuthal acoustic modes possess high Q values and high resonance frequencies, but have low cell constants. PA cells with high Q values are sensitive to long-term drifts (e.g., due to thermal expansion if the temperature is not carefully controlled), so that they require an active locking of the modulation frequency on the resonance frequency of the cell.

In a longitudinally excited resonator, a smaller acoustic gain, as a consequence of a relatively low Q value, is compensated for by the signal gain due to the smaller diameter.

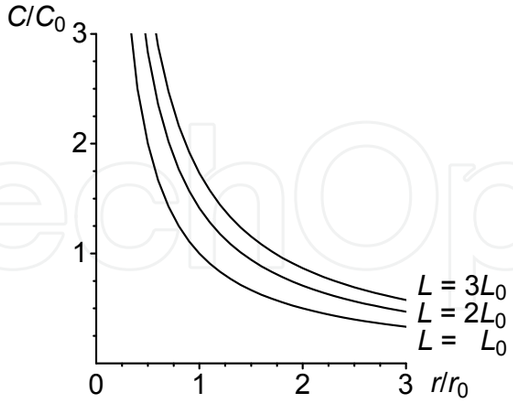


Fig. 6. Graphical representation of Eq. (26): dependence of the normalized cell constant on tube radius and resonator length.

According to Eqs. (24-26), to obtain a higher acoustic signal in a longitudinally excited resonator with a low Q-factor (a higher C), it is necessary to have a resonator with a large length and a small diameter. Yet, narrowing the tube diameter and increasing the tube length are restricted by the divergence of the laser beam over the length of the cell. The maximum length is limited by the minimum frequency at which the cell is to be operated or by the maximum absorption coefficient α_{max} that is to be detected ($L << 1/\alpha_{max}$). The minimum possible diameter is set by the beam diameter or the volume-to-surface ratio that is needed to minimize adsorption and desorption at the cell walls. A too small diameter of the PA cell gives rise to high PA background signals due to absorption of the wings of the gaussian laser beam profile. On the other hand, a high quality factor is required in order to decrease the background signal caused by window heating. In conclusion, the optimization of the PA cell geometry depends on the specific experimental conditions and the application for which it is designed.

3.8 Voltage signal

When the resonance contributions are included, the photoacoustic voltage signal can be obtained at a given operating frequency simply by multiplying the pressure response (Eq. 20) by the microphone responsivity ($V = pS_M$ and $\alpha_p = \alpha c$):

$$V = \alpha C S_M P_L c \ , \tag{27}$$

where: V (V) is the photoacoustic signal (peak-to-peak value); α (cm^{-1} atm^{-1}), the gas absorption coefficient at a given wavelength; C (Pa cm W^{-1}), the cell constant; S_M (V Pa^{-1}), the microphone responsivity; P_L (W), the cw laser power (unchopped value; 2x measured average value); and c (atm), the trace gas concentration (usually given in units of per cent, ppmV, ppbV or pptV). This equation reveals that the photoacoustic signal is linearly dependent on laser power. Thus, sensitive measurements benefit from using as much laser power as is reasonably available. Moreover, the signal is directly dependent on the number of molecules in the optical path (trace gas concentration), which means that this technique is

truly a "zero-baseline" approach, since no signal will be generated if the target molecules are not present.

Equation (27) is valid as long as absorption is small ($\alpha_p L << 1$), and the modulation frequency is higher than the inverse of the molecular diffusion time but lower than the inverse of the molecular relaxation time. The PA signal is linearly dependent on the absorption coefficient, cell constant, microphone responsivity, incident laser power, and absorbent trace gas concentration. Thus, by doubling Q (and consequently C), or the microphone responsivity, or the laser power, or the number of absorbing molecules in the optical path, the voltage will also double. The peak-to-peak value of the signal is obtained by multiplying by $2\sqrt{2}$ the rms voltage amplitude measured by the lock-in amplifier. As a rule, another parameter is used to characterize the PA cell, namely:

$$R = CS_M , \tag{28}$$

where R (V cm/W) is the (voltage) responsivity of the PA cell or the calibration constant. The cell constant C is multiplied by the responsivity of the microphone given in V/Pa units. A comparison of different PA cells can be made independently of the application in terms of this figure of merit. However, the cell characterization can be used only if a calibrated microphone is available. In this way, Eq. (27) becomes:

$$V = \alpha R P_L c . \tag{29}$$

To increase the detection sensitivity, we have to ensure: a) a cell constant as large as possible (optimization of the PA resonator); b) a large microphone responsivity; c) a laser power as high as possible, provided that saturation does not become a limiting factor; d) a narrow bandwidth of the lock-in amplifier, and e) a high absorption coefficient of the trace gas to be measured at the laser wavelength. It is also useful to increase the number n of microphones (connected in series), but this number is limited by the dimensions of the PA cell. The summation of the signals from the single microphones results in an n-times higher effective PA signal, because the total responsivity $S_{M\,tot}$ is increased n-fold, i.e.:

$$S_{M\,tot} = nS_M . \tag{30}$$

On the other hand, the incoherent noise only increases by $\sqrt{n}$. One thus obtains:

$$\mathrm{SNR}_{\mathrm{tot}} = \sqrt{n}\,\mathrm{SNR} . \tag{31}$$

The minimum measurable voltage signal $V = V_{min}$ is obtained at SNR = 1, where the minimum detectable concentration $c = c_{min}$ can be recorded:

$$c_{\min} = \frac{V_{\min}}{\alpha P_L R} . \tag{32}$$

The sensitivity of PA instruments increases with the laser power, as $V \propto \alpha P_L$. However, the voltage signal does not depend on the length of the absorption path. Furthermore, in contrast to other techniques based on absorption spectroscopy, the response of the acoustic detector is independent of the electromagnetic radiation wavelength as long as the absorption coefficient is fixed. According to theoretical considerations, extremely low

detection limits on the order of $\alpha_{min} = \alpha c_{min} \cong 10^{-10}$ cm^{-1} for 1 W incident laser power have been predicted (Sigrist, 1986) and experimentally proved (Harren et al., 1990). Such sensitivity makes it possible to detect many trace constituents in the sub-ppbV range. Theoretical calculations (see Section 2) predict the linearity of the signal response over a concentration range as broad as 7 orders of magnitude. This wide dynamic range, characteristic of LPAS, is important for air pollution monitoring, as it helps conduct measurements in polluted areas at the source (emission) as well as in rural areas (immission) (Sigrist et al., 1989).

3.9 Saturation effects

A PA signal may become saturated due to either a large concentration of the measured analyte or high laser power levels. We showed in Section 2 that, in the case of ethylene, the signal starts to saturate at a concentration of 65 ppmV. As a matter of fact, Thöny and Sigrist (Thöny & Sigrist, 1995) observed weak saturation effects on 10P(14) CO_2 laser transition for a concentration of 100 ppmV of ethylene. The degree of saturation is gas dependent. We found (Section 2.3) that a deviation of ~3% from linear behavior resulted in an optical density $\alpha Lc = 0.06$.

By increasing laser intensity, the excitation pumping rate of the molecules grows higher, and a molecule is more likely to absorb a nearby photon before it relaxes to the ground state. So, as the molecules in the excited state increase in numbers, the number of molecules which can absorb laser radiation is reduced. The gas actually becomes as though more transparent to laser radiation, and the effective absorption coefficient per unit laser power is lowered; this is called laser power saturation. Saturation due to nonlinear absorption of the laser power only occurs in focused high-power laser beams or when the PA cell is placed intracavity in a laser, so that the laser power can be on the order of tens of watts or even higher than 100 W. The pumping rate to a higher vibrational-rotational level is proportional to the laser light intensity; in the case of saturation it exceeds the collisional de-excitation rates.

Harren et al. (Harren et al., 1990) studied the saturation effects by placing the PA cell intracavity of a waveguide CO_2 laser. Extracavity, the ratio between 10P(14) and 10P(16) lines is 5.96 ± 0.2. Intracavity, this ratio becomes 2.8 ± 0.3 (47% from its extracavity value) at an intracavity laser power of 130 W (for a laser beam waist of 0.282 mm, that is at a laser intensity higher than 200 kW/cm^2). By lowering the intracavity laser power, this ratio increases to its extracavity value. This effect is caused by saturation of the transitions in C_2H_4 at the 10P(14) CO_2 laser line. Depletion from the vibrational excited level (ν_7) via other vibrational levels (e.g., ν_{10}) through collisions becomes slow in comparison with the pump rate due to the high intracavity power. When the laser beam waist is increased to 1.02 mm (laser intensity is decreased to 15.9 kW/cm^2), the ratio of the absorption coefficients of C_2H_4 on the 10P(14) and 10P(16) CO_2 laser lines increased to 4.7 ± 0.5 (78% of its extracavity value). To compensate for the saturation effect, these authors used an absorption coefficient of 23.7 cm^{-1}atm^{-1} (78% of 30.4 cm^{-1}atm^{-1} at an intracavity power of 100 W) for C_2H_4 at the 10P(14) CO_2 laser line.

By using an intracavity arrangement where the CO_2 laser power was varied between 10 and 70 W, Groot (Groot, 2002) measured the saturation parameter of ethylene for several laser lines. The relation of the effective absorption coefficient α_e to the intrinsic absorption coefficient α is given by $\alpha_e = \alpha/(1 + P/P_s)$, where P_s (W) is the laser power saturation

parameter and represents a measure for the relaxation rate. At $P = P_s$, the absorption coefficient decreases to half its initial value. The following values were obtained for P_s: 178 W at 10P(8) line; 102 W at 10P(10); 112 W at 10P(12); 51.8 W at 10P(14); 101 W at 10P(16); 128 W at 10P(18), and 112 W at 10P(20). The strongest saturation effect was observed at 10P(14) line, where the absorption coefficient is the largest. The saturation for this line at a laser power of 130 W corresponds to the equivalent absorption coefficient $\alpha_e = 0.285\alpha$. The stronger saturation in this case compared with the results of Harren et al. (Harren et al., 1990) could be accounted for by a tighter focusing of the laser beam (smaller beam waist). As a matter of fact, saturation is determined by the laser beam intensity (irradiance) rather than the laser power. Power saturation does not depend on the gas concentration in the PA cell (if the absorbing gas concentration is not too high).

4. Noises and limiting factors

4.1 Noises

In order to obtain an optimum SNR, noise control and interfering signals have to be taken into account (Dutu et al., 1994a; Dutu et al., 1994b). These limiting factors are discussed in the following two sections.

Noise plays an important role in all photoacoustic measurements and is of particular importance in the detection of ultralow gas concentrations, because the noise level limits the ultimate sensitivity. In the photoacoustic literature, the detection level is usually defined by the SNR, where the noise is given by the microphone signal measured with the laser light blocked. However, when light hits the PA cell, an additional background signal is generated which exists even when the absorbing species are not present in the detector. The background signal is often larger than the noise signal, and therefore the detection limit or sensitivity has to be defined by the signal-to-background ratio (SBR) in most experiments. Unfortunately, it is common practice to consider only the SNR. This procedure yields an extrapolated detection limit that may be far too small. The background signal is usually determined with a nonabsorbing gas, such as nitrogen, in the PA detector. It is influenced by many system properties, such as the pointing stability, the beam divergence, and the diameter of the laser beam.

For photoacoustic spectroscopy, "noise" often has a structure that is coherent with the signal from the target species, and therefore should more appropriately be treated as a background signal, not as noise. The background signal can be determined by measuring the acoustic signal in the absence of absorbers (i.e., with pure nitrogen), but with the same flow and in the same pressure conditions as those used for the sample gases.

The sensitivity-limiting factors which are encountered in LPAS can be classified into three categories:

a. Electrical noise, by which we mean any random fluctuation, whether electronic or acoustic, which does not have a fixed phase relation with the modulation of the laser intensity. It determines the ultimate detector sensitivity.
b. Coherent acoustic background noise, meaning a signal caused by the modulation process, but not attributable to the presence of the light beam in the PA cell. This signal is at the same frequency as, and locked in phase with respect to, the laser intensity modulation.

c. Coherent photoacoustic background signal. This signal, which is always present in the PA detector, is caused by the laser beam, yet not by light absorption in the bulk of the gas. Rather it is due to laser beam heating of the windows and of the absorbates at their surfaces, and heating of the PA resonator walls by the reflected or scattered light owing to imperfections of the focusing lens, windows and inner walls of the PA resonator. This signal is in phase with, and at the same frequency as, the laser intensity modulation. Therefore, it is not filtered out by the lock-in amplifier connected to the microphone. Thus, a background signal proportional to the laser power becomes the main factor that limits sensitivity.

The background signal in the PA cells may arise from several sources, some of which are listed below (Gerlach & Amer, 1980):

1. Window surface absorption: the molecules absorbed on the window surface and/or the window surface itself absorb the modulated laser radiation, and the resulting gas heating in the cell generates a pressure pulse.
2. Window bulk absorption: even the highest quality ZnSe window substrates exhibit a residual window absorption of ~10^{-3} cm^{-1}.
3. Off-axis radiation within the cell: light scattered from the windows and at the edge of the chopper blade may strike the inside walls of the PA resonator, where it may be absorbed and produce a signal.
4. Light scattering or absorption due to microaerosols.
5. Small amounts of contamination that may outgas from the cell materials, seals, and so forth.

The detection limit of the PA cell is determined by the combined effect of the intrinsic stochastic noise of the microphone, acoustic background noise, and photoacoustic background signal. Background signals are deterministic, and to the extent that they can be quantified and minimized, do not reduce the performance of the cell significantly. The detection limit is defined either at a signal-to-noise ratio of unity (SNR = 1) or at a signal-to-background ratio of unity (SBR = 1).

The amplifier input noise and microphone noise are gaussian in nature, that is, the amount of noise is proportional to the square root of the bandwidth in which the noise is measured. All of these noise sources are incoherent. The input noise of the SR830 lock-in amplifier used in our experiments is about 6 nV (rms)/ $\sqrt{\text{Hz}}$. Microphone noise, which is manifested as a noise voltage present at the microphone output terminals, can be expressed as a product between the normalized noise pressure value owing to both thermal agitation of the diaphragm and cartridge responsivity at the corresponding frequency and the square root of the measurement bandwidth. The electrical noise of Knowles EK models electret microphones is 40 nV (rms)/ $\sqrt{\text{Hz}}$. The overall random noise of multiple sources is determined by taking the square root of the sum of the squares of all the individual incoherent noise figures. For gaussian noise, the peak-to-peak value is about 5 times the rms noise value, while for the two other types of noises, the rms value must be multiplied by a factor of $2\sqrt{2} \cong 2.8$ to obtain the peak-to-peak amplitude. Electrical noise usually has a broadband frequency spectrum and can be reduced efficiently by narrowband filtering of the signal, as is done in the phase sensitive detection. A detection bandwidth of 0.25 Hz was set (a time constant of 1 second) in all of our measurements. Electrical noise can be reduced by using state-of-the-art (and therefore very expensive) lock-in amplifiers and/or by using longer time averaging (the noise decreases with the square root of the averaging time) at the cost of longer measurement times.

The two types of coherent background, however, are extremely narrowband signals at the same frequency as the modulation and hence cannot be filtered out. In addition, since the signal and the coherent photoacoustic background signal are both proportional to laser power, no improvement will be achieved as the laser power is increased.

Table 2 shows the magnitudes of these limiting factors in the case Brewster windows are used. We expressed each factor in several different sets of units (Dutu et al., 1994b): voltage, pressure amplitude, equivalent absorption coefficient that would give the same pressure amplitude, and the concentration of ethylene that would be required to give that much absorption.

Noise type	**Root-mean-square (rms) value**	**Equivalent pressure[a]**	**Equivalent absorption[b]**	**Equivalent C_2H_4 concentration[c]**
Electrical noise, V_N^e	0.15 μV/ $\sqrt{\text{Hz}}$	5.3x10^{-6} Pa/ $\sqrt{\text{Hz}}$	1.5x10^{-9} W cm^{-1}/ $\sqrt{\text{Hz}}$	4.9x10^{-11} W / $\sqrt{\text{Hz}}$
Coherent acoustic background noise[d], V_N^{ac}	2.6 μV	9.2x10^{-5} Pa	2.6x10^{-8} W cm^{-1} [f]	8.6x10^{-10} W [g]
Coherent photoacoustic background signal[e], V_N^b	2.7 μV/W	9.5x10^{-5} Pa/W	2.7x10^{-8} cm^{-1} [h]	8.9x10^{-10} [i]

[a] The equivalent peak-to-peak pressure was obtained by dividing the peak-to-peak noise level to microphone sensitivity: $2\sqrt{2}\ V_N^i / S_M$, where V_N^i is either V_N^e, V_N^{ac} or V_N^b (in our case, S_M = 8x10^{-2} V/Pa)
[b] The equivalent absorption was obtained by dividing the peak-to-peak noise level to cell responsivity: $2\sqrt{2}\ V_N^i / R$, where V_N^i is either V_N^e, V_N^{ac} or V_N^b (in our case, R = 280 V cm/W)
[c] The equivalent C_2H_4 concentration was obtained by dividing the equivalent absorption to the C_2H_4 absorption coefficient at one atmosphere pressure of the gas at the 10P(14) laser wavelength (α_p = 30.4 cm^{-1})
[d] We expressed the coherent acoustical background noise in V independent of the bandwidth, as did Gerlach and Amer (Gerlach & Amer, 1980) and Beck (Beck, 1985) (and not in V/ $\sqrt{Hz}$ as used by Harren et al. (Harren et al., 1990)); our measurements show that the acoustical background noise was independent of the lock-in bandwidth when the equivalent noise bandwidth (ENBW, the effective bandwidth for gaussian noise) of the low pass filter was varied between 0.08 Hz and 8 Hz (the lock-in time constant T was changed between 0.3 and 30 s, where ENBW = 1/(4T) for a slope of 6 dB/oct)
[e] The coherent photoacoustical background signal was measured in pure nitrogen at atmospheric pressure (1011 mbar) and at a temperature of 22°C: 12 μV at a laser power of 4.4 W for 10P(14) line of the CO_2 laser; this signal was the same both in a static gas or at a flow rate of 50 sccm (standard cubic centimeters per minute)
[f] The same as the limiting sensitivity of the cell, S_{cell}
[g] With a laser power P_L = 4.4 W, the minimum measurable concentration of ethylene was 0.2 ppbV, the same as the limiting measurable concentration of ethylene, c_{lim} (Table 2, Part II)
[h] The same as the minimum measurable absorption coefficient, α_{min} (Table 2, Part II)
[i] The same as the minimum detectable concentration, c_{min} (Table 2, Part II)

Table 2. Noises measured in our PA system.

The limiting electrical noise measured at resonance frequency was V_N^e = 0.15 μV / $\sqrt{\text{Hz}}$. At atmospheric pressure, the acoustic background noise was V_N^{ac} = 2.6 μV (at resonance frequency) under normal working conditions. A photoacoustic background signal of V_N^b (nitrogen) = 2.7 μV/W was observed, in phase and at resonance frequency, as the cell was filled with pure N_2 at atmospheric pressure.

To determine the actual levels of noises that would be observed in practice, the random electrical noise level of 0.15 μV/ $\sqrt{Hz}$, for example, must be multiplied by $B^{1/2}$. Also, to get

the noise-equivalent absorption one must multiply 1.5x10^{-9} W cm^{-1}/ $\sqrt{Hz}$ by $B^{1/2}P^{-1}$, where B is the bandwidth and P the laser power. In order to get an idea of the sensitivity that can be achieved for a representative trace gas, the equivalent ethylene concentration that would give the same signal level is also tabulated. To get the noise-equivalent ethylene concentration, multiply 4.9x10^{-11} W / $\sqrt{Hz}$ by $B^{1/2}P^{-1}$.

Our coherent acoustical background was 2.6 μV or 9.2x10^{-5} Pa, equivalent to an absorption of 2.6x10^{-8} W cm^{-1}. To get the equivalent absorption coefficient divide the latter number by P_L (5.9x10^{-9} cm^{-1}). This background signal is dependent on the location of the PA cell in relation to the sound sources associated with the modulation process.

The coherent photoacoustic background was 2.7 μV/W, or 9.6x10^{-5} Pa/W, assuming the beam was optimally aligned. This is equivalent to an absorption coefficient of 2.7x10^{-8} cm^{-1}, or an ethylene concentration of about 0.89 ppbV, independent of the laser power. Since the noise and coherent acoustical background can be made negligible by using high laser power, as is done in intracavity operation, the coherent photoacoustic background will be the ultimate limit of sensitivity.

In order to obtain a maximized SNR, a resonance frequency under 1 kHz is necessary. Under 1 kHz, the noise level is determined by the $1/f$ amplifier noise, showing a frequency behavior of $1/\omega$. Together with $C \propto \omega_0^{-1/2}$ (because $C \propto Q/\omega_0$, $Q \propto (d_v, d_h)^{-1}$ and $(d_v, d_h) \propto \omega_0^{-1/2}$, see Sections 3.6, 3.4 and 3.3), we get a SNR proportional to $\omega_0^{1/2}$. Above 1 kHz, where the $1/f$ amplifier noise is negligible, the SNR is proportional to $\omega_0^{-1/2}$.

Below 1 kHz, the $1/f$ amplifier noise is the main source. Above 1 kHz, the frequency independent Brownian noise takes over. Since the pressure amplitude is inversely proportional to the square root of the resonance frequency ($p \propto C$, Eq. 20), a convenient resonance can be found between 500 and 1500 Hz. This limits the choice to a cell length of 100-300 mm. If optimal signal enhancement were the only argument, one would rather choose a large (300 mm) resonator ($C \propto L^{1/2}$, Eq. 26). Shorter resonator lengths are necessary in the case of an intracavity setup due to the limited space inside the cavity. Also, a fast time response of the cell requires a short cell length.

When the sample gas is flown continuously through the detector, acoustical noise can be produced, if the gas flow is turbulent, if acoustical noise from the surroundings is coupled directly into the detector sample space or into the tubes connected to the detector and then propagated into the detector, or if acoustic disturbances from the pump running the sample gas through the detector are propagated through the tubes. Thick detector and tube walls, small flow rates, mounting of the cell and chopper in separate sound insulating boxes, etc. must be chosen to suppress these noise contributions.

The background signal can be minimized by placing the windows at nodes of the mode being excited and by introducing buffer volumes at both ends of the cell. The ratio of buffer to resonator diameters must be large enough, and the buffer length has to be equal to one-fourth of resonator length.

4.2 Gas interference

Interference of other absorbing substances may impair the theoretical detection limit in a multicomponent analysis of the real atmosphere. Such interference may be caused by other

molecular systems present in the environment or substances that are entrained by the carrier flux. If an interfering species is present in the environment, its effect can be minimized by either the introduction of scrubbers and cryogenic traps or the use of dual beam techniques using two PA cells. Sample-entrained interfering species present a more serious problem, since they will be present only near the source and therefore cannot be eliminated by dual beam spectroscopy.

In ambient air, one finds CO_2 concentrations of 330-365 ppmV (0.033%-0.0365%) (Sigrist, 1986; Harren et al., 1990; Rooth et al., 1990). This level may rise to about 1% in the practical conditions of an agricultural application. This poses a serious practical problem. The CO_2 molecule possesses absorption vibrational band transitions $v_1 \rightarrow v_3$ ($10^00 \rightarrow 00^01$) and $2v_2 \rightarrow v_3$ ($02^00 \rightarrow 00^01$) which are weak, while the lower levels are barely populated at room temperature (~1%). However, due to the exact coincidence of these vibrational-rotational transitions with the CO_2 laser lines and the relatively high concentration of CO_2 in comparison with trace gases like C_2H_4, carbon dioxide is inevitably excited by CO_2 laser radiation, and the related photoacoustic signal may exceed the trace signal by many orders of magnitude. The absorption coefficient increases strongly with temperature, but is independent of the CO_2 concentration over a wide range. A 1.5% concentration of CO_2 has an absorption strength comparable to 1 ppmV of C_2H_4 (for CO_2 at the 10P(14) laser line, $\alpha(CO_2) = 2.1\text{x}10^{-3}$ atm^{-1}cm^{-1} and $c(C_2H_4) = c(CO_2)\alpha(CO_2)/\alpha(C_2H_4) = 10^{-6}$ atm = 1 ppmV). At the 10P(14) line of CO_2, 360 ppmV of CO_2 has an absorption coefficient equal to that of 24.8 ppbV of C_2H_4. Similarly, at the 9R(30) line of CO_2 at 21°C, the same concentration of CO_2 has an absorption coefficient equal to that of 13.5 ppbV of NH_3. Water vapor exhibits a broad continuum with occasional weak lines in the frequency range of the CO_2 laser (for H_2O at the 10P(14) laser line, $\alpha(H_2O) = 2.85\text{x}10^{-5}$ atm^{-1}cm^{-1}). The two dominant peaks are the absorption lines on 10R(20) and the most favorable for ambient air measurement, the 10P(40) laser transition. The absorption of 1% of water vapor in air (50% relative humidity at 18°C) is about the same as that of 9.4 ppbV of C_2H_4 at the 10P(14) line or 5 ppbV of NH_3 at the 9R(30) line of CO_2 (Rooth et al., 1990). However, at a constant temperature the absorption coefficient $\alpha(H_2O)$ depends on the water vapor concentration x and appears to obey the relation: $\alpha(H_2O) = \alpha_0 x$, where α_0 is a constant. The natural unpolluted atmosphere contains H_2O at a concentration level of ~1.5%.

Ammonia (a colorless, poisonous gas with a characteristic smell and well solvable in water) is vibrationally excited to the ν_2 state, usually by means of the $saR(5, K)$ transitions at λ = 9.22 μm. These levels can be excited by the 9R(30) line of the CO_2 laser, where the absorption coefficient $\alpha(NH_3)$ has a value of 56 cm^{-1} atm^{-1} (Rooth et al., 1990). Ammonia is present in the atmosphere in concentrations ranging from below 0.1 ppbV over open water up to several tens of ppbV in areas with intensive livestock breeding.

Due to the additive character of the photoacoustic signal under normal atmospheric conditions, the presence of a large amount of water vapor and carbon dioxide impedes C_2H_4 detection in the low-concentration range (ppbV). Consequently, some means of selective spectral discrimination is required if ethylene is to be detected interference free in the matrix of absorbing gases. There are several ways to overcome this problem. The first is to remove CO_2 from the flowing sample by absorption on a KOH (potassium hydroxide)-based scrubber inserted between the sampling cell and the PA cell (a specific chemical reaction results: KOH $\rightarrow$ K_2CO_3 and water). In this way, concentrations below 1 ppmV CO_2 (equivalent to a concentration of 0.07 ppbV of C_2H_4) can be achieved without influencing the C_2H_4 concentration.

Another method is a multicomponent analysis approach. The PA spectrum of an arbitrary gas mixture is represented by a linear combination of the absorption spectra of all constituents. Hence, the absorption spectra of all expected constituents that contribute to the total absorption have to be determined prior to the analysis of a multicomponent gas mixture. Let us assume a nitrogen atmosphere including a mixture of n absorbing gases at unknown concentration levels c_1, c_2, ... , c_n, low enough to assure linearity. The PA signal $V(\lambda)$ of the n absorbing compounds j (j = 1, 2, ... , n) with their concentration c_j and their wavelength-dependent absorption coefficients $\alpha_j(\lambda)$ is the sum of the individual signals from each compound. In some cases, the calculation becomes more complicated due to different phases of photoacoustic signals generated by the individual constituents of the mixture. For some components, e.g. CO_2, a temporal delay in the production of the PA signal may occur. This effect is known as kinetic cooling and results in a phase shift of the PA signal. So, the PA signal has to be considered as the vector sum of the individual signals from each compound:

$$V(\lambda) = \sum_{j=1}^{n} V_j(\lambda) = RP_L(\lambda) \sum_{j=1}^{n} c_j \alpha_j(\lambda), \tag{33}$$

where R (V cm/W) is the cell responsivity. By sequentially tuning the laser to m different wavelengths (discrete CO_2-laser transitions) λ_i, i = 1, 2, ... , m, we obtain m measured photoacoustic signals V_i from which we derive a set of m linear equations for the unknown concentration levels c_j:

$$V_i(\lambda_i) = RP_i \sum_{j=1}^{n} \alpha_{ij}(\lambda_i) c_j = \sum_{j=1}^{n} a_{ij} c_j, \tag{34}$$

where $P_i = P_L(\lambda_i)$, $a_{ij} = RP_i\alpha_{ij}$ (a constant for a given gas, a given wavelength and a given laser power), and $m \geq n$ (it should be noted that the system of linear equations is only well defined if the number m of laser transitions is higher than the number of gas components j); α_{ij} is the absorption coefficient of the j-th trace absorbant gas at wavelength λ_i, while P_i is the laser power at that wavelength. The measurements result in PA signals V_i from all components j in the gas mixture which absorb on the wavelength of the laser transition, λ_i. The minimum number of measurements at different laser wavelengths must be equal to at least the number of unknown trace gases, $m = n$. In this case we can define:

$$B = \begin{pmatrix} b_{11} \dots b_{1n} \\ \vdots \quad \vdots \\ b_{n1} \dots b_{nn} \end{pmatrix} = \begin{pmatrix} a_{11} \dots a_{1n} \\ \vdots \quad \vdots \\ a_{n1} \dots a_{nn} \end{pmatrix}^{-1}. \tag{35}$$

Therefore,

$$c_j = \sum_{i=1}^{n} b_{ji} V_i. \tag{36}$$

for j = 1, 2, ... , n. The coefficients b_{ji} have units of atm V^{-1}. If the number m of CO_2 laser lines used to carry out the analysis of a gas mixture is equal to or higher than the number n of absorbing components in the sample (whose CO_2 laser absorption coefficients are known), the unknown concentrations of each n component can be determined with the proper

selection of laser lines. The solution of sets of simultaneous equations is generally required to estimate the concentrations of each species in a multicomponent mixture and select the optimal wavelengths for a fixed number of laser lines. The selection of CO_2 laser wavelengths for the optimum detection of a single species in the presence of interferences can usually be carried out by comparing the corresponding laser absorption profiles.

This method was used by Perlmutter et al. (Perlmutter et al., 1979), who observed a minus sign of the calculated CO_2 concentration level. The minus sign stems from the fact that the absorption coefficients of CO_2 were taken to be positive in the numerical analysis. Actually the absorption coefficients of CO_2 present in nitrogen at low concentration levels (up to ~0.5%), at CO_2 laser transitions, are of negative sign. The absolute values are unchanged. This minus sign is associated with the kinetic cooling effect. They found experimentally that in a longitudinal resonant PA cell (chopping frequency = 1 kHz) the CO_2 gives a $180^o \pm 10^o$ out-of-phase PA signal relative to operation with normal gases like ethylene. This is true when CO_2 is present at concentration levels up to ~0.5% in nitrogen. At concentration levels higher than ~0.5%, the kinetic cooling phase deviation does not exceed ~180^o and highly depends on concentration, thus leading to an increasing PA signal level.

A crucial feature of photoacoustics on gas mixtures is the molecular dynamics involved in the conversion of internal molecular energy to heat (Olaffson et al., 1989; Henningsen et al., 1990). This is particularly important when dealing with mixtures involving CO_2 and N_2. The near degeneracy between the fundamental asymmetric stretch of CO_2 (2349 cm^{-1}) and the N_2 v = 1 vibration (2331 cm^{-1}) leads to a large cross section for resonant energy transfer. In a CO_2 laser, this mechanism is used to advantage by adding N_2 to the gas mixture in order to increase the pump rate by energy transfer from the vibrationally excited N_2 to CO_2 in the ground state. In our case, the situation is reversed. Thus, following absorption of CO_2 laser radiation, an excited CO_2 molecule transfers its excitation energy to N_2, where it resides for a long time owing to the metastable character of the excited N_2 levels (the lifetime of the vibrational level v = 1 is ≅ 1 ms at 1 atm; 1 atm = 101.325 kPa). Since the CO_2 molecule was initially taken out of an excited state, and the transition was a hot band transition, there now is a non-equilibrium situation among the CO_2 vibrational levels, and equilibrium is eventually restored at the expense of translational energy. Thus, following radiation absorption, a transient cooling of the CO_2 gas takes place, and the effect is therefore referred to as kinetic cooling. In trace gas detection, this means that the photoacoustic phase of the CO_2 signal will be significantly different from the phase of the trace gas signal, where no kinetic cooling is involved. The situation is further complicated if water is present in the gas mixture, since water molecules are effective in deexciting the metastable N_2 levels and hence in reducing the phase contrast. The presence of 1% water vapors speeds up the relaxation of vibrationally excited N_2, and this effect reduces the phase contrast to about 135^o down from 180^o. This phase contrast is a very important aid in the analysis of mixtures where one of the components is strongly dominant, since a quantitative analysis of the phase contrast may provide information about the H_2O concentration.

The presence of H_2O and CO_2 will always influence the measurement of C_2H_4 and NH_3 concentrations. These background gases absorb CO_2 laser radiation and produce simultaneously occurring photoacoustic signals. A comparison of the predicted amplitude and phase of the photoacoustic signal with experimental data is given in Fig. 7 (Rooth et al., 1990).

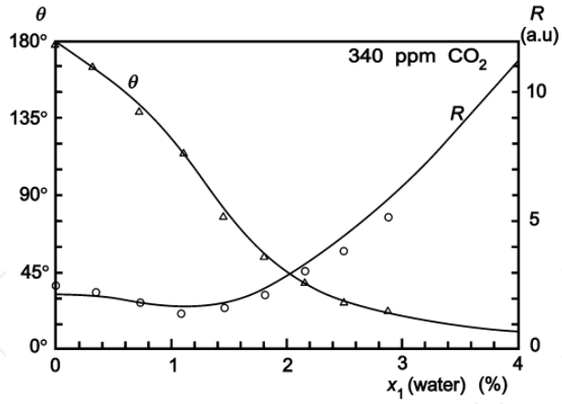


Fig. 7. Predicted amplitude R and phase θ for air with 340 ppmV CO_2 as a function of water vapor concentration. The corresponding experimental data are plotted for a frequency of 560 Hz and an excitation at 9R(28) CO_2 line (9.23 μm) (Rooth et al., 1990).

In Fig. 8, the phase of the calculated heat production rate for a CO_2 – N_2 – O_2 – H_2O mixture is plotted as a function of the concentrations c_{CO_2} and c_{H_2O} [19]. The data used for this plot were those for 10R(20) CO_2 laser transition, i.e., I_0 = 20 W/cm², σ_{H_2O} = 3.5x10^{-23} cm² and σ_{H_2O} = 1.0x10^{-22} cm², and a chopper frequency f = 2650 Hz. As demonstrated in Fig. 8, the phase reversal only occurs within rather narrow concentration ranges. Thus, a heat-rate phase different from 0° or 180° is rarely expected for low H_2O and CO_2 concentrations.

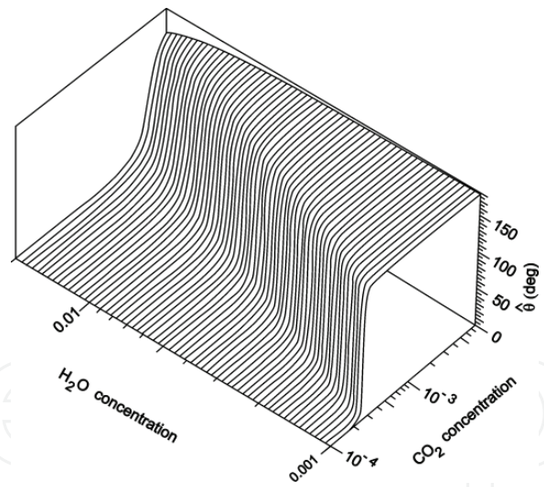


Fig. 8. Calculated phase of heat production rate for a CO_2 – N_2 – O_2 – H_2O mixture as function of the concentrations c_{CO_2} and c_{H_2O} and for c_{N_2} = 0.8 and c_{O_2} = 0.2 (Meyer & Sigrist, 1990).

The multicomponent analysis can utilize the phase information of the photoacoustic response to suppress the CO_2 signal. A high concentration of CO_2 yields a phase shift of the signal with respect to the acoustic signal of ethylene. A combined signal for a CO_2-C_2H_4 mixture is less than the sum of both individual amplitudes (vectorially added). The zero phase of the two-phase vector lock-in amplifier is adjusted to pure C_2H_4 absorption, and thus a mixture of CO_2 and C_2H_4 in air is measured on two CO_2 laser transitions. One obtains four pieces of information, i.e. the CO_2-C_2H_4 mixture phase shift and absorption coefficients

for both lines. From this, with known absorption coefficients for both lines, the CO_2 and C_2H_4 concentrations can be extracted (Rooth et al., 1990). A good estimate is obtained from the difference between the two measured signals V_a and V_b. Putting $V_a = R_a \exp(i\theta_a)$ and $V_b = R_b \exp(i\theta_b)$ the magnitude of the difference is found with the cosine rule:

$$|V_a - V_b| = \left[R_a^2 + R_b^2 - 2R_a R_b \cos(\theta_a - \theta_b)\right]^{1/2}. \tag{37}$$

Here it is only the difference between the two phase angles that is required, so absolute calibrations can be avoided. This approach has the advantage that a high laser power can be used, and no partial failure of the scrubber can falsify the C_2H_4 concentration.

In a multicomponent mixture, this effect can be taken into account by measuring the amplitudes V_i of the PA signal at the laser transitions i as well as its phases θ_i, where the number i = 1... m stands for the discrete CO_2 laser transitions with the powers $P(\lambda_i) = P_i$. Thus, similar to Eq. (34) we have the following equation for the PA signal amplitude:

$$V_i \cos\theta_i = RP_i \sum_{j=1}^{n} c_j \alpha_{ij}(\lambda_i) \cos\theta_{ij}, \tag{38}$$

with i =1... m, j = 1... n, $n \le m$, where c_j is the concentration of the gas component j and α_{ij} is the absorption coefficient of the gas compound j at the laser transition i. The phase θ_{ij} is a mathematical aid for easy calculation. It is nearly independent of the laser transition i for a certain gas component and can thus be written as θ_j. In our wavelength range it is only CO_2 which shows a phase $\theta_j = \pi$, whereas all the other gases studied so far show a phase $\theta_j = 0$. In real measurements small deviations of the phases from the predicted ones occur due to measurement errors. Nevertheless, the approximation $\theta_{ij} = \theta_j = 0$ for all the other air compounds is well justified. It should be noted that the system of linear equations is only well defined if the number of gas components j is smaller than the number m of laser transitions, i.e., for $n \le m$. Based on measurements of the signals V_i, phases θ_j, and laser powers P_i, and knowing the absorption coefficients α_{ij} from literature data or calibration measurements, the unknown concentrations c_j can be derived by solving the above equation system. The algorithm of the data analysis has been described by Meyer and Sigrist (Meyer & Sigrist, 1990). For multicomponent mixtures an algorithm, e.g., a nonlinear Levenberg-Marquardt fit (Moeckli et al., 1998) is employed to fit the measured spectrum on the basis of calibration spectra of the individual compounds.

The concentrations of C_2H_4, CO_2, and H_2O in nitrogen at atmospheric pressure can be determined by measuring the PA signals using three CO_2 laser transitions, e.g., 10P(14), 10P(20) and 10R(20) (Sigrist et al., 1989). The 10P(14) and 10R(20) transitions coincide with sharp peaks of the IR spectra of C_2H_4 (α = 30.4 $cm^{-1}atm^{-1}$) and H_2O (α = 8.36x10^{-4} $cm^{-1}atm^{-1}$), respectively. The 10P(20) line that is used to measure CO_2 concentration (α = 2.2x10^{-3} $cm^{-1}atm^{-1}$) could be replaced by many other transitions without much change in sensitivity, because CO_2 is relatively spectrally flat.

Rooth et al. (Rooth et al., 1990) determined the H_2O, CO_2, and NH_3 contents in ambient air by using four laser transitions (10R(20) is used to compute water vapor concentration using the absorption coefficient at the actual gas temperature; the influence of the CO_2 absorption on the measurement of H_2O is also taken into account by using the 9R(18) and 9R(28) lines;

the difference in the two signals yields the CO_2 concentration with the help of Eq. (37); the fourth line, 9R(30) together with 9R(28) provides the NH_3 concentration). Nägele and Sigrist (Nägele & Sigrist, 2000) recorded the PA signal on two transitions for each compound, carefully selected for maximum absorption, minimum absorption interference, and good laser performance. In addition, they measured the PA signal on two laser transitions (10P(12), 10P(40)), for which all of the investigated gases exhibit negligible absorption, to verify the constant background signal. Therefore, the spectra to monitor ethylene (10P(14), 10P(16)), ethanol (9P(8), 9P(32)), methanol (9P(34), 9P(36)), and CO_2 (10P(20), 9R(20)) comprise ten different transitions. Thus cross references are possible and the background signal, which is the same for these lines, can be subtracted. This extension to several laser lines yields better detection limits and selectivity, although the time for one full measurement increases with the number of lines.

5. Conclusions

Based on previous discussion, PA spectroscopy, performed with tunable CO_2 lasers as radiation sources, offers the following main characteristics relevant to *in situ* trace gas monitoring:

i. Its high sensitivity makes it possible to measure absorption coefficients on the order of 10^{-8} cm^{-1}, corresponding to densities of $\mu g/m^3$ or concentrations of ppbV (10^{-9} atm) for most substances;
ii. The PA cell responsivity is independent of radiation wavelength;
iii. A large number of gases and vapors are measurable with the same instrument;
iv. It has high selectivity, meaning that it can clearly distinguish among various compounds;
v. The experimental setup is rather simple, immune to interference, and, for example, does not require cryogenic cooling of the IR detectors, etc.;
vi. Relative portability for *in situ* measurements (carried on mobile trailers in the troposphere or on balloon-borne systems to the stratosphere);
vii. Operational simplicity and real time data analysis make it capable of performing quasi continuous measurements;
viii. The calibration with certified gases and gas mixtures is straightforward and reliable;
ix. Detection linearity and a wide dynamic range of at least 6 orders of magnitude are offered (from several fractions of ppbV to tens of ppmV), i.e., the same apparatus can be used for low (immission) and high (emission) concentrations.
x. Specially designed PA cells can perform continuous measurements on flowing gas mixtures, i.e., a much better temporal resolution can be achieved than the one provided by, *inter alia*, gas chromatography.

The outstanding features of the PA cell, most importantly its small size, simplicity, and robustness, cannot be fully utilized unless it is combined with a suitable laser source. The recent commercial availability of sealed-off, medium-power (50 W), grating-tunable CO_2 lasers has paved the way to the development of instrumentation with excellent sensitivity and compact footprints that can be readily deployed in industrial or medical settings. Further improvements are possible by using resonant PA cells with high Q factors (limited, though, by fluctuations of the modulation frequency), multipass, or intracavity arrangements.

Other laser sources were successfully applied in photoacoustic spectroscopy. Recent developments in compact near-infrared (NIR) and IR all-solid-state tunable lasers, such as the tunable semiconductor lasers, quantum-cascade lasers, and devices utilizing non-linear

optical mixing in non-linear crystals (OPOs, difference frequency generators (DFGs), optical parametric amplifiers (OPAs)), have significantly advanced the application of photoacoustic techniques in sensitive trace gas analysis.

NIR diode lasers are becoming more and more popular due to recent development of cheap high-quality, compact sources having a spectral emission which falls in the absorption range of many molecules of great practical interest. The range of the available NIR diode lasers spans from about 0.8 to 2.1 μm. Many gases like methane, acetylene, CO, and CO_2 exhibit overtone absorptions in the 1.55-1.65 μm wavelength region which can be covered by a conventional external cavity diode laser (ECDL). Detection limits are lower compared with measurements in the fundamental absorption region but still sufficient for many applications. A combination of diode lasers with PA detection was used by various authors to detect ammonia (Fehér et al., 1994; Schmohl et al., 2002), methane (Schäfer et al., 1998), elemental carbon (Petzold et al., 1995), toluene (Beenen et al., 1998), and water vapor (Bozóki et al., 1999). Different experimental arrangements such as external cavity diode lasers (Sneider et al., 1997) or intracavity PA cells (Bozóki et al., 1996) were tested. At present, 1.6 μm diode lasers, coinciding with the first vibrational overtones and combination bands of molecules containing a CH bond, are those that – in the NIR range – provide the best trade-off between cost and molecular detection efficiency (Boschetti et al., 2002).

Recent progress with quantum-cascade lasers makes them attractive sources in the important 3- to 5-μm spectral range. This area is important not only because the characteristic absorption bands of, among others, CO, N_2O, HCl and CH_2O, lie herein, but also because there is an atmospheric transparent window in this range. Soon after the first appearance of these lasers, gas monitoring applications using various detection schemes were reported (Sharpe et al., 1998; Kosterev et al., 2008). Quantum-cascade lasers were used to detect ammonia and water vapor at 8.5 μm (Paldus et al., 1999), NO at 5.2 μm (Menzel et al., 2001), $^{12}CH_4$, $^{13}CH_4$ and N_2O isotopomers at 8.1 μm (Gagliardi et al., 2002), trace gases (CH_4, N_2O, H_2O) in laboratory air at 7.9 μm (Kosterev & Tittel, 2002), carbon dioxide, methanol and ammonia at 10.1/10.3 μm (Hofstetter et al., 2001), CH_4 and NO at 7.9 μm and 5.3 μm (Grossel et al, 2006; Grossel et al., 2007) and simultaneously CO and SO_2 at 4.56 μm and 7.38 μm (Liu et al., 2011). In contrast to semiconductor (diode) lasers, quantum-cascade lasers are unipolar light sources based on only one type of carrier, usually electrons, making intraband transitions between confined energy levels within the conduction band. The term "cascade" comes from the fact that the confined energy levels are arranged the way of a waterfall, so that electrons undergoing lasing transitions travel from one stage to the next, just like water does in a multiple-step water cascade. Therefore, one electron can emit sequentially up to n photons when n steps are present. The emission wavelength of a quantum-cascade laser is determined not by the semiconductor bandgap but by the quantum confinement in the quantum wells created by the quantum-well material and the barrier material. Therefore, quantum-cascade lasers can span a wide wavelength range using the same material system. Quantum-cascade lasers with wavelengths from 3.5 to 13 μm have been fabricated by use of the same material system (InGaAs wells and InAlAs barriers).

Widely tunable, narrowband optical parametric oscillator (OPO)-based laser sources were used for trace gas spectroscopy in the fundamental C-H stretch vibration region (3-5 μm) (Bohren et al., 1997), to detect ethane at 3.34 μm (Kühnemann et al., 1998; van Herpen et al., 2002), N_2O at 2.86 μm (Costopoulos et al., 2002), or methane at 3.39 μm (Miklós et al., 2002). Most of today's commercial OPOs are based on BaB_2O_4 crystals (BBO) pumped by the third

harmonic of a Nd:YAG laser and their IR tuning range is limited to approximately 2 μm. Difference frequency generation (DFG) is certainly the most promising technique for the extension of the tuning range of an existing tunable laser to the mid IR (2.5-4.5 μm) (Fischer & Sigrist, 2002). Spectrometers using DFG were applied to monitoring, for example, formaldehyde in ambient air at 3.53 μm (Rehle et al., 2001) and volcanic gases (CH_4, CO_2, HCl, SO_2, H_2O vapor) at 3.3-4.4 μm (Richter et al., 2002).

6. References

Angeli, G.Z.; Solyom, A.M.; Miklos, A. & Bicanic, D.D. (1992). Calibration of a Windowless Photoacoustic Cell for Detection of Trace Gases. *Anal. Chem.,* Vol.64, No.2, (January 1992), pp. 155-158, ISSN 0003-2700

Beck, S.M. (1985). Cell Coatings to Minimize Sample (NH_3 and N_2H_4) Adsorption for Low-Level Photoacoustic Detection. *Appl. Opt.,* Vol.24, No.12, (June 1985), pp. 1761-1763, ISSN 0003-6935

Beenen, A. & Niessner, R. (1998). Development of Photoacoustic Gas Sensor for In-Situ and On-Line Measurement of Gaseous Water and Toluene. *Analyst,* Vol.123, No.4, pp. 543-545, ISSN 0003-2654

Bell, A.G. (1880). On the Production and Reproduction of Sound by Light. *Am. J. Sci.,* Vol.XX, pp. 305-324

Bell, A.G. (1881). Upon the Production of Sound by Radiant Energy. *Phil. Mag. J. Sci.*, Vol.XI, pp. 510-528

Bernegger, S. & Sigrist, M.W. (1987). Longitudinal Resonant Spectrophone for CO-laser Photoacoustic Spectroscopy. *Appl. Phys. B,* Vol.44, No.2, (October 1987), pp. 125-132, ISSN 0946-2171

Bicanic, D. (Ed.) (1992). *Photoacoustic and Photothermal Phenomena III*, Springer Series in Optical Sciences, Vol.69, Springer, ISBN 978-0-387-55669-9, Berlin, Germany

Bijnen, F.G.; Reuss, J. & Harren, F.J.M. (1996). Geometrical Optimization of a Longitudinal Resonant Photoacoustic Cell for Sensitive and Fast Trace Gas Detection. *Rev. Sci. Instrum.,* Vol.67, No.8, (August 1996), pp. 2914-2923, ISSN 0034-6748

Bohren, A. & Sigrist, M.W. (1997). Optical Parametric Oscillator Based Difference Frequency Laser Source for Photoacoustic Trace Gas Spectroscopy in the 3 μm Mid-IR Range. *Infrared Phys. Technol.,* Vol.38, No.7, (December 1997), pp. 423-435, ISSN 1350-4495

Boschetti, A.; Bassi, D.; Iacob, E.; Iannotta, S.; Ricci, L. & Scotoni, M. (2002). Resonant Photoacoustic Simultaneous Detection of Methane and Ethylene by Means of a 1.63-μm Diode Laser. *Appl. Phys. B,* Vol.74, No.3, (February 2002), pp. 273-278, ISSN 0946-2171

Bozóki, Z.; Sneider, J.; Gingl, Z.; Mohácsi, A.; Szakáll, M. & Szabó, G. (1999). A High-Sensitivity, Near- Infrared Tunable-Diode-Laser-Based Photoacoustic Water-Vapor-Detection System for Automated Operation. *Meas. Sci. Technol.,* Vol.10, No.11, (November 1999), pp. 999-1003, ISSN 0957-0233

Bozóki, Z.; Sneider, J.; Szabó, G.; Miklós, A.; Serényi, M.; Nagy, G. & Fehér, M. (1996). Intracavity Photoacoustic Gas Detection with an External Cavity Diode Laser. *Appl. Phys. B,* Vol.63, No.4, (October 1996), pp. 399-401, ISSN 0946-2171

Bruce, C.W. & Pinnick, R.G. (1977). In Situ Measurements of Aerosol Absorption with a Resonant cw Laser Spectrophone. *Appl. Opt.,* Vol.16, No.7, (July 1977), pp. 1762-1765, ISSN 0003-6935

Costopoulos, D.; Miklós, A. & Hess, P. (2002). Detection of N_2O by Photoacoustic Spectroscopy with a Compact, Pulsed Optical Parametric Oscillator. *Appl. Phys. B,* Vol.75, No.2-3, (September 2002), pp. 385-389, ISSN 0946-2171

Cristescu, S.; Dumitras, D.C. & Dutu, D.C.A. (2000). Characterization of a Resonant Cell Using the Acoustic Transmission Line Model. *Proc. SPIE SIOEL '99: Sixth Symposium on Optoelectronics,* Vol.4068, T. Necsoiu, M. Robu, D.C. Dumitras (Eds.), pp. 263-272, SPIE, ISBN 978-0-819-43705-1, Bellingham, WA, USA

Cristescu, S.; Dumitras, D.C.; Dutu, D.C.A. & Mujat, C. (1997). Real-Time Detection System for Laser Photoacoustic Applications. *Rom. Rep. Phys.,* Vol.49, No.8-9-10, pp. 757-768, ISSN 1221-1451

Dewey Jr. C.F.; Kamm, R.D. & Hackett, C.E. (1973). Acoustic Amplifier for Detection of Atmospheric Pollutants. *Appl. Phys. Lett.,* Vol.23, No.11, (December 1973), pp. 633-635, ISSN 0003-6951

Dewey, C.F. (1977). Design of Optoacoustic Systems. In *Optoacoustic Spectroscopy and Detection*, Ch. 3, Y.-H. Pao (Ed.), 47-77, Academic, ISBN 978-0-125-44159-9, New York, NY, USA

Dumitras, D.C.; Dutu, D.C.; Matei, C.; Magureanu, A.M.; Petrus, M. & Popa, C. (2007a). Improvement of a Laser Photoacoustic Instrument for Trace Gas Detection. *U. P. B. Sci. Bull., Series A,* Vol.69, No.3, pp. 45-56, ISSN 1223-7027

Dumitras, D.C.; Dutu, D.C.; Matei, C.; Magureanu, A.M.; Petrus, M. & Popa, C. (2007b). Laser Photoacoustic Spectroscopy: Principles, Instrumentation, and Characterization. *J. Optoelectr. Adv. Mater.,* Vol.9, No.12, (December 2007), pp. 3655-3701, ISSN 1454-4164

Dutu, D.C.A.; Cristescu, S. & Dumitras, D.C. (1994b). Measurement of Photoacoustic Signal and Noises in a Sensitive Spectrophone with a Frequency Stabilized CO_2 Laser. In *Proc. SPIE ROMOPTO'94-Fourth Conference in Optics,* Vol.2461, V.I. Vlad (Ed.), pp. 308-316, SPIE, ISBN 978-0-819-41813-5, Bellingham, WA, USA

Dutu, D.C.A.; Dumitras, D.C.; Cristescu, S. & Sarkozy, L. (1994a). Evaluation of Photoacoustic Signal and Noises in a Sensitive Spectrophone Irradiated by a CO_2 Laser Beam. *Rom. Rep. Phys.,* Vol.46, No.7-8, pp. 639-644, ISSN 1221-1451

Fehér, M.; Jiang, Y.; Maier, J.P. & Miklós, A. (1994). Optoacoustic Trace-Gas Monitoring with Near-Infrared Diode Lasers. *Appl. Opt.,* Vol.33, No.9, (March 1994), pp. 1655-1658, ISSN 0003-6935

Fischer, C. & Sigrist, M.W. (2002). Trace-Gas Sensing in the 3.3-μm Region Using a Diode-Based Difference-Frequency Laser Photoacoustic System. *Appl. Phys. B,* Vol.75, No.2-3, (September 2002), pp. 305-310, ISSN 0946-2171

Gagliardi, G.; Tamassia, F.; De Natale, P.; Gmachl, C.; Capasso, F.; Sivco, D.L.; Baillargeon, J.N.; Hutchinson, A.L. & Cho, A.Y. (2002). Sensitive Detection of Methane and Nitrous Oxide Isotomers Using a Continuous Wave Quantum Cascade Laser. *Eur. Phys. J. D,* Vol.19, No.3, (June 2002), pp. 327-331, ISSN 1434-6060

Gerlach, R. & Amer, N.M. (1978). Sensitive Optoacoustic Detection of Carbon Monoxide by Resonance Absorption. *Appl. Phys. Lett.,* Vol.32, No.4, (February 1978), pp. 228-231, ISSN 0003-6951

Gerlach, R. & Amer, N.M. (1980). Brewster Window and Windowless Resonant Spectrophones for Intracavity Operation. *Appl. Phys.A,* Vol.23, No.3, (November 1980), pp. 319-326, ISSN 0947-8396

Gondal, M.A. (1997). Laser Photoacoustic Spectrometer for Remote Monitoring of Atmospheric Pollutants. *Appl. Opt.,* Vol.36, No.15, (May 1997), pp. 3195-3201, ISSN 1559-128x

Groot, T. (2002). *Trace Gas Exchange by Rice, Soil and Pears. A Study Based on Laser Photoacoustic Spectroscopy*, PhD Thesis, University of Nijmegen, ISBN 978-9-090-15380-2, Nijmegen, The Netherlands

Grossel, A.; Zeninari, V.; Joly, L.; Parvitte, B.; Courtois, D. & Durry, G. (2006). New Improvements in Methane Detection Using a Helmholtz Resonant Photoacoustic Laser Sensor: A Comparison Between Near-IR Diode Lasers and Mid-IR Quantum Cascade Lasers. *Spectrochim. Acta A,* Vol.63, No.5, (April 2006), pp. 1021-1028, ISSN 1386-1425

Grossel, A.; Zeninari, V.; Joly, L.; Parvitte, B.; Durry, G. & Courtois, D. (2007). Photoacoustic Detection of Nitric Oxide with a Helmholtz Resonant Quantum Cascade Laser Sensor. *Infrared Phys. Technol.,* Vol.51, No.2, (October 2007), pp. 95-101, ISSN 1350-4495

Gusev, V.E. & Karabutov, A.A. (1993). *Laser Optoacoustics*, American Institute of Physics, ISBN 978-1-563-96036-9, Melville, NY, USA

Harren, F.J.M. & Reuss, J. (1997). Spectroscopy, Photoacoustic, In *Encyclopedia of Applied Physics*, Vol.19, G.L. Trigg (Ed.), 413-435, VCH Publishers, ISBN 978-3-527-40478-0, New York, USA

Harren, F.J.M.; Bijnen, F.G.C.; Reuss, J.; Voesenek, L.A.C.J. & Blom, C.W.P.M. (1990). Sensitive Intracavity Photoacoustic Measurements with a CO_2 Waveguide Laser. *Appl. Phys. B,* Vol.50, No. 2, (February 1990), pp. 137-144, ISSN 0946-2171

Harren, F.J.M.; Cotti, G.; Oomens, J. & te Lintel Hekkert, S. (2000). Photoacoustic Spectroscopy in Trace Gas Monitoring, In *Encyclopedia of Analytical Chemistry*, Vol.3, R.A. Meyers (Ed.), 2203-2226, Wiley, ISBN 978-0-471-97670-7 Chichester, UK

Henningsen, J.; Olaffson, A. & Hammerich, M. (1990). Trace Gas Detection with Infrared Gas Lasers. In *Applied Laser Spectroscopy*, W. Demtröder, M. Inguscio (Eds.), 403-416, Plenum Press, ISBN 978-0-306-43717-1, New York, NY, USA

Hess, P. (1983). Resonant Photoacoustic Spectroscopy, In *Topics in Current Chemistry*, Vol.111, F.L. Boschke (Ed.), 1-32, Springer, ISBN 3-540-16403-0, Berlin, Germany

Hess, P. (Ed.). (1989). *Photoacoustic, Photothermal and Photochemical Processes in Gases*, Topics in Current Physics, Vol.46, Springer, ISBN 978-0-387-51392-2, Berlin, Germany

Hofstetter, D.; Beck, M.; Faist, J.; Nägele, M. & Sigrist, M.W. (2001). Photoacoustic Spectroscopy with Quantum Cascade Distributed-Feedback Lasers. *Opt. Lett.,* Vol.26, No.12, (June 2001), pp. 887-889, ISSN 0146-9592

Hubert, M.H. (1983). *Laser Optoacustic Detector Measurement of Signatures of a Selection of Environmental Contaminants.* Rep. No. 83-715-1, Ultra Lasertech Inc., Mississauga, Canada

Johnson, R.H.; Gerlach, R.; Thomas III, L.J. & Amer, N.M. (1982). Loss Mechanisms in Resonant Spectrophones. *Appl. Opt.,* Vol.21, No.1, (January 1982), pp. 81-89, ISSN 0003-6935

Kaiser, R. (1959). On the Theory of the Spectrophone. *Can. J. Phys.,* Vol.37, No.12, (December 1959), pp. 1499-1513, ISSN 0008-4204

Kamm, R.D. (1976). Detection of Weakly Absorbing Gases Using a Resonant Optoacoustic Method. *J. Appl. Phys.*, Vol.47, No.8, (August 1976), pp. 3550-3558, ISSN 0021-8979

Kerr, E.L. & Atwood, J. (1968). The Laser Illuminated Absorptivity Spectrophone: A Method for Measurement of Weak Absorptivity in Gases at Laser Wavelengths. *Appl. Opt.,* Vol.7, No.5, (May 1968), pp. 915-921, ISSN 0003-6935

Kosterev, A.A. & Tittel, F.K. (2002). Chemical Sensors Based on Quantum Cascade Lasers. *IEEE J. Quantum Electron.,* Vol.38, No.6, (June 2002), pp. 582-591, ISSN 0018-9197

Kosterev, A.A., Wysocki, G.; Bakhirkin, Y.A.; So, S.; Lewicki, R.; Fraser, M.; Tittel, F. & Curl, R.F. (2008). Application of Quantum Cascade Lasers to Trace Gas Analysis. *Appl. Phys. B,* Vol.90, No.2, (February 2008), pp. 165-176, ISSN 0946-2171

Kreuzer, L.B. & Patel C.K.N. (1971). Nitric Oxide Air Pollution: Detection by Optoacoustic Spectroscopy. *Science*, Vol.173, No.3991, (July 1971), pp. 45-47, ISSN 0036-8075

Kreuzer, L.B. (1971). Ultralow Gas Concentration Infrared Absorption Spectroscopy. *J. Appl. Phys.,* Vol.42, No.7, (June 1971), pp. 2934-2943, ISSN 0021-8979

Kreuzer, L.B. (1977). The Physics of Signal Generation and Detection. In *Optoacoustic Spectroscopy and Detection*, Ch.1, Y.-H. Pao (Ed.), 1-25, Academic, ISBN 978-0-125-44150-9, New York, NY, USA

Kreuzer, L.B.; Kenyon, N.D. & Patel, C.K.N. (1972). Air Pollution: Sensitive Detection of Ten Pollutant Gases by Carbon Monoxide and Carbon Dioxide Lasers. *Science*, Vol.177, No.4046, (July 1972), pp. 347-349, ISSN 0036-8075

Kritchman, E.; Shtrikman, S. & Slatkine, M. (1978). Resonant Optoacoustic Cells for Trace Gas Analysis. *J. Opt. Soc. Am.,* Vol.68, No.9, (September 1978), pp. 1257-1271, ISSN 1084-7529

Kühnemann, F.; Schneider, K.; Hecker, A.; Martis, A.A.E.; Urban, W.; Schiller, S. & Mlynek, J. (1998). Photoacoustic Trace-Gas Detection Using a cw Single-Frequency Parametric Oscillator. *Appl. Phys. B,* Vol.66, No.6, (June 1998), pp. 741-745, ISSN 0946-2171

Liu, W.; Wang, L.; Li, L.; Liu, J.; Liu, F.-Q. & Wang, Z. (2011). Fast Simultaneous Measurement of Multi-Gases Using Quantum Cascade Laser Photoacoustic Spectroscopy. *Appl. Phys. B,* Vol.103, No.3, (June 2011), pp. 743-747, ISSN 0946-2171

Mandelis, A. & Hess, P. (Eds.) (1997). *Progress in Photothermal and Photoacoustic Science and Technology*, Vol.3, SPIE Press Book, ISBN 978-0-819-42450-1, Bellingham, WA, USA

Mandelis, A. (Ed.) (1992). *Progress in Photothermal and Photoacoustic Science and Technology*, Vol.1, Elsevier, ISBN 978-0-819-42450-1, New York, USA

Mandelis, A. (Ed.) (1994). *Progress in Photothermal and Photoacoustic Science and Technology*, Vol.2, Prentice Hall, ISBN 978-0-131-47430-8, Englewood Cliffs, NJ, USA

Menzel, L.; Kosterev, A.A.; Curl, R.F.; Titel, F.K.; Gmachl, C.; Capasso, F.; Sivco, D.L.; Baillargeon, J.N.; Hutchinson, A.L.; Cho, A.Y. & Urban, W. (2001). Spectroscopic Detection of Biological NO with a Quantum Cascade Laser. *Appl. Phys. B,* Vol.72, No.7, (May 2001), pp. 859-863, ISSN 0946-2171

Meyer, P.L. & Sigrist, M.W. (1990). Atmospheric Pollution Monitoring Using CO_2-Laser Photoacoustic Spectroscopy and Other Techniques. *Rev. Sci. Instrum.,* Vol.61, No.7, (July 1990), pp. 1779-1807, ISSN 0034-6748

Miklós, A.; Hess, P. & Bozoki, Z. (2001). Application of Acoustic Resonators in Photoacoustic Trace Gas Analysis and Metrology. *Rev. Sci. Instrum.* Vol.72, No.4, (April 2001), pp. 1937-1955, ISSN 0034-6748

Miklós, A.; Lim, C.-H.; Hsiang, W.-W.; Liang, G.-C.; Kung, A.H.; Schmohl, A. & Hess, P. (2002). Photoacoustic Measurement of Methane Concentrations with a Compact Pulsed Optical Parametric Oscillator. *Appl. Opt.,* Vol.41, No.15, (May 2002), pp. 2985-2993, ISSN 0003-6935

Moeckli, M.A.; Hilbes, C. & Sigrist, M.W. (1998). Photoacoustic Multicomponent Gas Analysis Using a Levenberg-Marquardt Fitting Algorithm. *Appl. Phys. B,* Vol.67, No.4, (October 1998), pp. 449-458, ISSN 0946-2171

Morse, P.M. & Ingard, K.U. (1986). *Theoretical Acoustics*, Princeton University Press, ISBN 978-0-691-02401-4, Princeton, NJ, USA

Olaffson, A.; Hammerich, M.; Bülow, J. & Henningsen, J. (1989). Photoacoustic Detection of NH_3 in Power Plant Emission with a CO_2 Laser. *Appl. Phys. B,* Vol.49, No.2, (August 1989), pp. 91-97, ISSN 0946-2171

Paldus, B.A.; Spence, T.G.; Zare, R.N.; Oomens, J.; Harren, F.J.M.; Parker, D.H.; Gmachl, C.; Cappasso, F.; Sivco, D.L.; Baillargeon, J.N.; Hutchinson, A.L. & Cho, A.Y. (1999). Photoacoustic Spectroscopy Using Quantum-Cascade Lasers. *Opt. Lett.,* Vol.24, No.3, (February 1999), pp. 178-180, ISSN 0146-9592

Pao, Y.-H. (Ed.) (1977). *Optoacoustic Spectroscopy and Detection*, Academic, ISBN 978-0-125-44150-6, New York, USA

Patel, C.K.N. & Tam, A.C. (1981). Pulsed Optoacoustic Spectroscopy of Condensed Matter. *Rev. Mod. Phys.,* Vol.53, No.3, (July-September 1981), pp. 517-554, ISSN 0034-6861

Perlmutter, P.; Shtrikman, S. & Slatkine, M. (1979). Optoacoustic Detection of Ethylene in the Presence of Interfering Gases. *Appl. Opt.,* Vol.18, No.13, (July 1979), pp. 2267-2274, ISSN 0003-6935

Petzold, A. & Niessner, R. (1995). Novel Design of a Resonant Photoacoustic Spectrophone, for Elemental Carbon Mass Monitoring. *Appl. Phys. Lett.,* Vol.66, No.10, (March 1995), pp. 1285-1287, ISSN 0003-6951

Preece, W.H. (1881). On the Conversion of Radiant Energy into Sonorous Vibrations. *Proc. R. Soc.,* Vol.31, pp. 506-520

Pushkarsky, M.B.; Weber, M.E.; Baghdassarian, O.; Narasimhan, L.R. & Patel, C.K.N. (2002). Laser-Based Photoacoustic Ammonia Sensors for Industrial Applications. *Appl. Phys. B*, Vol.75, No.4-5, (April 2002), pp. 391-396, ISSN 0946-2171

Rehle, D.; Leleux D.; Erdelyi, M.; Tittel, F.; Fraser, M. & Friedfeld, S. (2001). Ambient Formaldehyde Detection with a Laser Spectrometer Based on Difference-Frequency Generation in PPLN. *Appl. Phys. B,* Vol.72, No.8, (June 2001), pp. 947-952, ISSN 0946-2171

Reid, J.; Shewchun, J.; Garside, B.K. & Balik, E.A. (1978). High Sensitivity Pollution Detection Employing Tunable Diode Lasers. *Appl. Opt.*, Vol.17, No.2, (January 1978), pp. 300-307, ISSN 0003-6935

Richter, D.; Erdelyi, M.; Curl, R.F.; Tittel, F.K.; Oppenheimer, C.; Duffell, H.J. & Burton, M. (2002). Field Measurements of Volcanic Gases Using Tunable Diode Laser Based Mid-Infrared and Fourier Transform Infrared Spectrometers. *Opt. Lasers Eng.,* Vol.37, No.2-3, (March 2002), pp. 171-186, ISSN 0143-8166

Röntgen, W.C. (1881). Über Töne, welche durch intermittierende Bestralung eines Gases entstehen. *Ann. der Phys. und Chem.,* Vol.1, pp. 155-159

Rooth, R.A.; Verhage, A.J.L. & Wouters, L.W. (1990). Photoacoustic Measurement of Ammonia in the Atmosphere: Influence of Water Vapor and Carbon Dioxide. *Appl. Opt.,* Vol.29, No. 25, (September 1990), pp. 3643-3653, ISSN 0003-6935

Rosencwaig, A. (1980). *Photoacoustics and Photoacoustic Spectroscopy*, Chemical Analysis Vol.57, Wiley, ISBN 978-0-471-04495-4, New York, USA

Schäfer, S.; Mashni, M.; Sneider, J.; Miklós, A.; Hess, P.; Pitz, H.; Pleban, K.-U. & Ebert, V. (1998). Sensitive Detection of Methane with a 1.65 μm Diode Laser by

Photoacoustic and Absorption Spectroscopy. *Appl. Phys. B,* Vol.66, No.4, (April 1998), pp. 511-516, ISSN 0946-2171

Schmid, T. (2006). Photoacoustic Spectroscopy for Process Analysis. *Anal. Bioanal. Chem.,* Vol.384, No.5, (March 2006), pp. 1071-1086, ISSN 1618-2642

Schmohl, A.; Miklós, A. & Hess, P. (2002). Detection of Ammonia by Photoacoustic Spectroscopy with Semiconductor Lasers. *Appl. Opt.*, Vol.41, No.9, (March 2002), pp. 1815-1823, ISSN 0003-6935

Sharpe, S.W.; Kelly, J.F.; Hartman, J.S.; Gmachl, C.; Capasso, F.; Sivco, D.L.; Baillargeon, J.N. & Cho, A.Y. (1998). High-Resolution (Doppler-Limited) Spectroscopy Using Quantum-Cascade Distributed-Feedback Lasers. *Opt. Lett.,* Vol.23, No.7, (September 1998), pp. 1396-1398, ISSN 0146-9592

Sigrist, M.W. (1986). Laser Generation of Acoustic Waves in Liquids and Gases. *J. Appl. Phys.,* Vol.60, No.7, (October 1986), pp. R83-R121, ISSN 0021-8979

Sigrist, M.W. (2003). Trace Gas Monitoring by Laser Photoacoustic Spectroscopy and Related Techniques. *Rev. Sci. Instrum.,* Vol.74, No.1, (January 2003), pp. 486-490, ISSN 0034-6748

Sigrist, M.W. (Ed.) (1994). *Air Monitoring by Spectroscopic Techniques*, Vol.127, Wiley Chemical Analysis Series, Wiley, ISBN 978-0-471-55875-3, New York, USA

Sigrist, M.W.; Bernegger, S. & Meyer, P.L. (1989). Atmospheric and Exhaust Air Monitoring by Laser Photoacoustic Spectroscopy, In *Topics in Current Physics* "*Photoacoustic, Photothermal and Photochemical Processes in Gases*", Ch.7, Vol.46, P. Hess (Ed.), 173-211, Springer, ISBN 978-3-540-51392-2, Berlin, Germany

Sneider, J.; Bozóki, Z.; Szabó, G. & Bor, Z. (1997). Photoacoustic Gas Detection Based on External Cavity Diode Laser Light Sources. *Opt. Eng.,* Vol.36, No.2, (February 1997), pp. 482-486, ISSN 0091-3286

Tam, A.C. (1986). Applications of Photoacoustic Sensing Techniques. *Rev. Mod. Phys.,* Vol.58, No.2, (April-June 1986), pp. 381-431, ISSN 0034-6861

Terhune, R.W. & Anderson, J.E. (1977). Spectrophone Measurements of the Absorption in Visible Light by Aerosols in the Atmosphere. *Opt. Lett.*, Vol.1, No.2, (August 1977), pp. 70-72, ISSN 0146-9592

Thomas III, L.J.; Kelly, M.J. & Amer, N.M. (1978). The Role of Buffer Gases in Optoacoustic Spectroscopy. *Appl. Phys. Lett.,* Vol.32, No.11, (June 1978), pp. 736-738, ISSN 0003-6951

Thöny, A. & Sigrist, M.W. (1995). New Developments in CO_2-Laser Photoacoustic Monitoring of Trace Gases. *Infrared Phys. Technol.,* Vol.36, No.2, (February 1995), pp. 585-615, ISSN 1350-4495

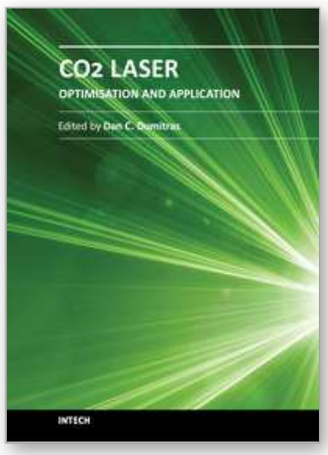
Tonelli, M.; Minguzzi, P. & Di Lieto, A. (1983). Intermodulated Optoacoustic Spectroscopy. *J. Physique (Colloque C6),* Vol.44, No.10, (October 1983), pp. 553-557, ISSN 0449-1947

Tyndall, J. (1881). Action of an Intermittent Beam of Radiant Heat upon Gaseous Matter. *Proc. R. Soc.*, Vol.31, pp. 307-317

van Herpen, M.; te Lintel Hekkert, S.; Bisson, S.E.; Harren, F.J.M. (2002). Wide Single-Mode Tuning of a 3.0-3.8-μm, 700-mW, Continuous Wave Nd:YAG-Pumped Optical Parametric Oscillator Based on Periodically Poled Lithium Niobate. *Opt. Lett.,* Vol.27, No.8, (April 2002), pp. 640-642, ISSN 0146-9592

West, G.A. (1983). Photoacoustic Spectroscopy. *Rev. Sci. Instrum.,* Vol.54, No.7, (July 1983), pp. 797-817, ISSN 0034-6748

Zharov, V.P. & Letokhov, V.S. (1986). *Laser Optoacoustic Spectroscopy*, Vol.37, Springer, ISBN 978-3-540-11795-4, Berlin, Germany



CO2 Laser - Optimisation and Application

Edited by Dr. Dan C. Dumitras

ISBN 978-953-51-0351-6
Hard cover, 436 pages
Publisher InTech
Published online 21, March, 2012
Published in print edition March, 2012

The present book includes several contributions aiming a deeper understanding of the basic processes in the operation of CO2 lasers (lasing on non-traditional bands, frequency stabilization, photoacoustic spectroscopy) and achievement of new systems (CO2 lasers generating ultrashort pulses or high average power, lasers based on diffusion cooled V-fold geometry, transmission of IR radiation through hollow core microstructured fibers). The second part of the book is dedicated to applications in material processing (heat treatment, welding, synthesis of new materials, micro fluidics) and in medicine (clinical applications, dentistry, non-ablative therapy, acceleration of protons for cancer treatment).

How to reference

In order to correctly reference this scholarly work, feel free to copy and paste the following:

Dan C. Dumitras, Ana Maria Bratu and Cristina Popa (2012). CO2 Laser Photoacoustic Spectroscopy: I. Principles, CO2 Laser - Optimisation and Application, Dr. Dan C. Dumitras (Ed.), ISBN: 978-953-51-0351-6, InTech, Available from: http://www.intechopen.com/books/co2-laser-optimisation-and-application/co2-laser-photoacoustic-spectroscopy-i-principles

INTECH
open science | open minds

InTech Europe
University Campus STeP Ri
Slavka Krautzeka 83/A
51000 Rijeka, Croatia
Phone: +385 (51) 770 447
Fax: +385 (51) 686 166
www.intechopen.com

InTech China
Unit 405, Office Block, Hotel Equatorial Shanghai
No.65, Yan An Road (West), Shanghai, 200040, China
中国上海市延安西路65号上海国际贵都大饭店办公楼405单元
Phone: +86-21-62489820
Fax: +86-21-62489821

© 2012 The Author(s). Licensee IntechOpen. This is an open access article distributed under the terms of the Creative Commons Attribution 3.0 License, which permits unrestricted use, distribution, and reproduction in any medium, provided the original work is properly cited.

IntechOpen

IntechOpen